Gas sensors based on ceramic *p-n* heterocontacts

by

Seymen Murat Aygun

A thesis submitted to the graduate faculty

in partial fulfillment of the requirements for the degree of

MASTER OF SCIENCE

Major: Materials Science and Engineering

Program of Study Committee:
David P. Cann, Major Professor
Keith Woo
Xiaoli Tan

Iowa State University

Ames, Iowa

2005

Graduate College
Iowa State University

This is to certify that the master's thesis of

Seymen Murat Aygun

has met the thesis requirements for Iowa State University

Major Professor

For the Major Program

TABLE OF CONTENTS

CHAPTER 1. INTRODUCTION 1
1.1 Background 1
1.1.1 Semiconductor Gas Sensors: Historical Perspective 1
1.1.2 Basic Working Principles and the Role of Catalysis 2
1.1.3 Parameters that Determine the Sensor Performance 8
1.1.4 Smart Gas Sensors 11
1.2 Heterocontact Gas Sensors 11
1.2.1 *p-n* Junctions 11
1.2.1.1 No Applied Bias 12
1.2.1.2 Forward and Reverse Biases 14
1.2.1.3 *p-n* Junction Band Diagrams 19
1.2.1.4 Depletion Layer Capacitance 21
1.2.1.5 Reverse Breakdown 21
1.2.2 *p-n* Heterojunctions 22
1.2.3 Use of *p-n* Heterojunctions as Gas Sensors 24

CHAPTER 2. EXPERIMENTAL PROCEDURES 32
2.1 Material Preparation 32
2.2 Property Measurements 33
References 35

CHAPTER 3. HYDROGEN SENSITIVITY OF DOPED CuO/ZnO HETEROCONTACT SENSORS 37
Abstract 37
1. Introduction 38
2. Experimental 39
2.1 Sample Preparation and Phase Analyses 39
2.2 Electrical Characterization 40
3. Results and Discussions 41
3.1 Microstructure and Phase Analyses 41
3.2 Dopant Effects on Electrical Properties and Sensor Response 42
4. Summary and Conclusions 44
Acknowledgements 46
References 46
Tables and Figures 49

CHAPTER 4. RESPONSE KINETICS OF DOPED CuO/ZnO HETEROCONTACTS 59
Abstract 59
1. Introduction 60
2. The Model 62

3. Experimental 63
4. Results and Discussion 64
5. Summary and Conclusions 68
Acknowledgments 69
References and Notes 69
Tables and Figures 70

CHAPTER 5. GENERAL CONCLUSIONS 79

ACKNOWLEDGEMENTS 82

CHAPTER 1. INTRODUCTION

1.1 Background

1.1.1 *Semiconductor Gas Sensors: Historical Perspective*

In 1950's it was discovered that the electrical properties of some metal oxides are changed when they are exposed to reducing gases, especially at elevated temperatures [1, 2]. By applying this phenomenon, in 1962 Seiyama *et al.* proposed the idea of gas sensing using ZnO thin films [3]. The other commonly used sensor material, SnO_2, was proposed as a gas sensor in the same year by Taguchi [4], and since 1968 these sensors have been commercially available through Figaro Engineering [5]. The Taguchi Gas Sensor is a partially sintered SnO_2 bulk device whose resistance in air is very high and drops when exposed to reducing gases such as combustibles (H_2, CO, CH_4, C_3H_8) or volatile organic vapors and it has enjoyed a substantial popularity because of its ease of fabrication and stability relative to other competitive systems such as polymers and organic films. In addition to research on understanding the fundamentals of the sensing mechanism, the studies on SnO_2 sensors have been directed on enhancing the sensor performance through the addition of noble metals (Pt, Pd, etc.), synthesis of thick and thin film sensors, and doping with other semiconductors [6-14]. Other metal oxides such as Fe_2O_3, TiO_2, WO_3 and Co_3O_4 have also been used as gas sensors. Despite these broad studies in the semiconductor sensor area, problems such as insufficient gas selectivity, inability to detect very low gas concentrations, and degradation of the sensor performance by surface contamination still persist. Thus, there is a growing need for chemical sensors with novel properties.

1.1.2 *Basic Working Principles and the Role of Catalysis*

In semiconductors, because of the non-stoichiometry of the material, lattice defects arise along with electrons or holes associated with these defects that provide the conductivity. Semiconductor sensors detect gases via variations in their conductance due to the change in the concentration of these charge carriers. The most widely accepted explanation of the operation principle, in *n*-type SnO_2 involves a conductivity change observed in a normal atmosphere, due to the interaction between adsorbed oxygen and the defect electrons. The effect of the reducing gas is to perturb this equilibrium, thereby changing the conductivity [15]. Oxygen adsorbates on the surface can be of several forms: O_2, O_2^-, O^-, O^{2-}. The lattice oxygen O_o^x can also be reactive with the incoming reducing agent. However, the lattice oxygen is tightly bonded in n-type metal oxides. Among these different oxygen species, O^- is the most active form which can easily react with reducing gases. As shown in Figure 1.1, the adsorption of oxygen on the surface extracts conduction electrons from the near-surface region forming an electron depleted surface layer which results in an electric field and a

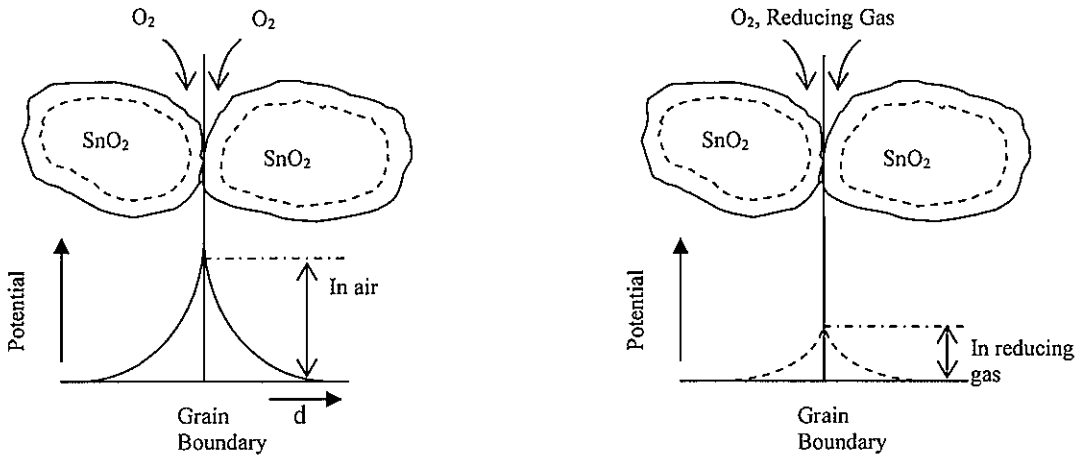

Figure 1.1: Model of inter-grain potential barrier.

potential barrier associated with this electric field. This barrier is indicated as eV_s, where V_s is dependent upon the concentration of adsorbed oxygen. The density of electrons with sufficient energy to cross this barrier is n_s, given by the Boltzmann equation [16]:

$$n_s = N_d \exp(\frac{-eV_s}{k_B T}) \tag{1.1}$$

where N_d is the density of donors. The more oxygen present on the surface, the higher the potential barrier and fewer electrons can overcome the potential barrier leading to a higher resistance. When a reducing gas is introduced, adsorbed oxygen is consumed by reacting with the reducing gas, and the entrapped electrons are returned to the oxide grains resulting in a decrease of the potential barrier and the resistance. The reaction on the surface can be written as:

$$\frac{1}{2}O_2 + e^- \xrightarrow{SnO_2} O_{ad}^- \tag{1.2}$$

$$R + O_{ad}^- \xrightarrow{SnO_2} RO + e^- \tag{1.3}$$

A steady state equilibrium between these two reactions determines the amount of adsorbed O^- on the surface, which, in turn, determines V_s and through equation (1.1) the conductivity. When there is no reducing gas present in the atmosphere, reaction (1.2) leads to a very high concentration of O^- on the SnO_2 surface and a very low conductance. As the concentration of the reducing gas increases, the concentration of the O^- decreases and therefore the conductivity increases.

Metal oxide sensors are directly related to the phenomenon of catalysis. These sensors are essentially catalysts since they increase the rate of a reaction without being consumed in the process. They achieve this by providing an alternative path involving

different activated complexes, with effectively a lower activation energy than the uncatalyzed mechanism [17]. Figure (1.2) shows the energetics of catalyzed and uncatalyzed reaction [15]:

$$A + B \leftrightarrow C + D \tag{1.4}$$

The uncatalyzed reaction is characterized by very high activation energy E_g. In the catalyzed reaction the gaseous species A and B adsorb on the surface with an exothermic heat of adsorption ΔH_{ads}, (state I). The state I is followed by state II toward the reaction products C and D characterized by the activation energy E_c, which is much lower than E_g.

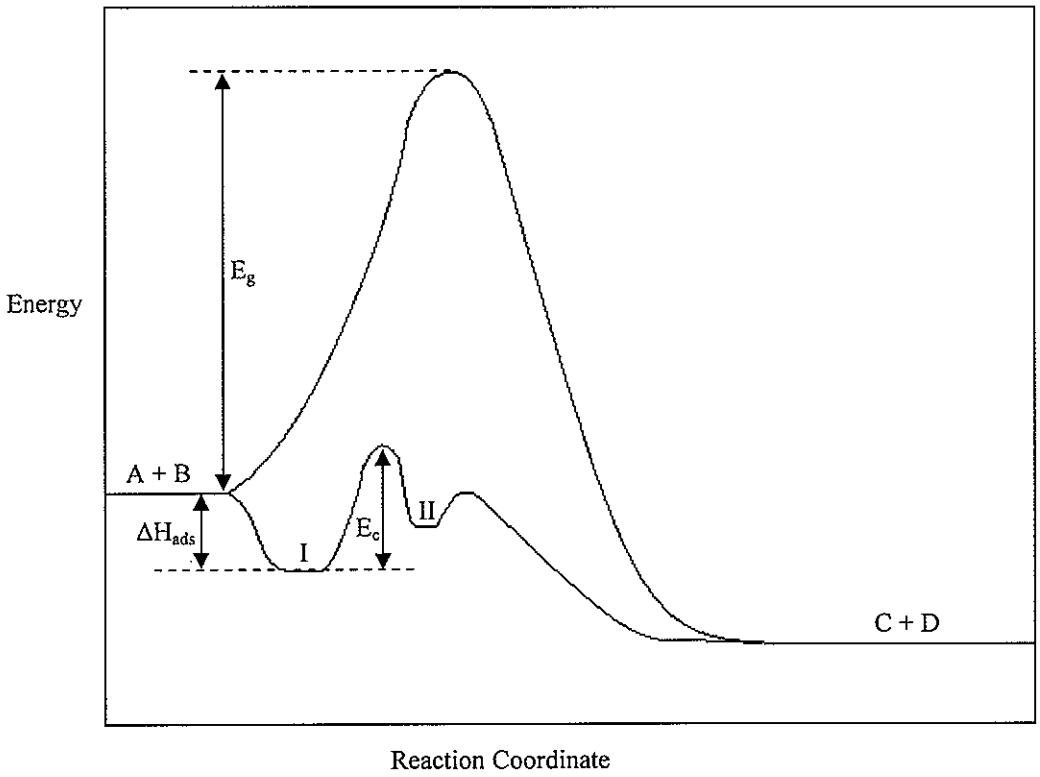

Figure 1.2: Surface energy profile for the Reaction (1.4), uncatalyzed and catalyzed reactions (modified from Gentry and Jones [15]).

From Figure (1.2) it can also be seen that as the heat of adsorption (ΔH_{ads}) becomes more negative, i.e. species are too strongly adsorbed, the activation energy for the catalytic reaction E_c also increases. However, it is important to note that the activation energy is not the only factor determining the activity of the catalyst. For example, as the heat of adsorption becomes more positive, and thus the activation energy decreases the surface concentration of the adsorbates will decrease. As a result, although the reaction becomes energetically favorable, fewer species will be available for reaction. As proposed by Gentry and Jones, there are two key steps in the catalytic activity of the metal oxide gas sensors [15]:

i. Adsorption of the gases onto the solid surface

ii. Reaction between the adsorbed species and/or with the solid surface

Atoms or ions on the surface of the solid cannot fully satisfy their valency and coordination requirements. This leads to a certain permanent force acting towards the bulk. Consequently, the driving force for the solid to adsorb the gaseous species is to reduce its surface energy. If this attraction is weak gas adsorption is due to van der Waals forces, (i.e. physisorption), and is characterized by low heats of adsorption resulting in weak catalytic activity (Figure 1.2). On the other hand, if the solid has a high surface energy the gas may become adsorbed through an exchange of electrons with the surface, i.e. chemical bonds are formed, this is called chemisorption. The nature of the bonds may be covalent or ionic, and in both cases the heats of adsorption are large. Typically heats of physisorption are ~15 kcal/mol, and that of chemisorption are >15 kcal/mol [18]. Chemisorption can lead to new reaction paths with different energetics from those of the gas phase reaction and thus provides the necessary conditions for heterogeneous catalysis. Although physisorption does not provide the conditions for catalysis, it can be and often is a precursor to chemisorption.

In a semiconductor gas sensor, to detect the concentration of a gas phase via changes in its conductivity, the conductivity change must be proportional to the gas phase concentration to be sensed. To understand this relationship, the kinetics of adsorption and reaction must be considered. The adsorption isotherm can be expressed using a basic model, Langmuir theory of adsorption:

$$\theta_A = \frac{b_A P_A}{1 + b_A P_A} \tag{1.5}$$

Here, the surface coverage θ_A is related to the partial pressure of the gas P_A. The term b_A is the equilibrium constant for adsorption, i.e., the ratio of the rate constants for adsorption and desorption, and is a function of the heat of adsorption. Two important assumptions are made in this model. First, the adsorption is terminated upon completion of a monomolecular adsorbed gas layer ($0 \leq \theta_A \leq 1$). Second, the heat of adsorption does not vary with coverage. The first assumption arises from the assertion that any gas molecule that strikes an adsorbed atom must reflect from the surface. The second assumption requires a homogeneous surface and non-interacting adsorbed species. Although the model is physically unrealistic for describing the adsorption of gases on real surfaces, and there are modified isotherms [18], it may still be used to predict the qualitative relationship between gas concentration and surface coverage. For the simple case of one gas adsorbing on the catalyst surface, from Equation (1.5), if $b_A P_A$ is small, the coverage is proportional to P_A, and hence conductivity changes can be used to measure gas concentration. On the other hand, if $b_A P_A >> 1$, then the coverage will approximate to unity and the catalyst will become insensitive to coverage.

If there are two species adsorbed on the surface, then the Equation (1.5) becomes [15]:

$$\theta_A = \frac{b_A P_A}{1 + b_A P_A + b_B P_B} \qquad \text{and} \qquad \theta_B = \frac{b_B P_B}{1 + b_A P_A + b_B P_B} \tag{1.6}$$

If $b_B P_B >> b_A P_A$, then the Equations (1.6) reduce to

$$\theta_A = \frac{b_A P_A}{1 + b_B P_B} \qquad \text{and} \qquad \theta_B = \frac{b_B P_B}{1 + b_B P_B} \tag{1.7}$$

If $b_B P_B$ is also $>>1$, the Equations (1.7) become

$$\theta_A \approx \frac{b_A P_A}{1 + b_B P_B} \qquad \text{and} \qquad \theta_B \approx 1 \tag{1.8}$$

These equations tell us that, if the conductivity is dependent on the weakly adsorbed species A, one can measure either the concentration of A or B. However, if conductivity is dependent on the strongly adsorbed species B, surface coverage approximates to unity becoming independent of gas concentration.

If reaction between adsorbed species occurs, the relative coverages can further be displaced from the original equilibrium. The reaction rate can be written as:

$$rate = k\theta_A\theta_B \tag{1.9}$$

Therefore, the rate of the reaction between the species will depend on the adsorption rates of the species. Again the suitability of these processes for gas detection will depend on which species dominates conduction changes. For example, on n-type semiconductors the coverage of oxygen is very low (θ_A in Equation 1.8), whereas a reducing gas will have a very high coverage (θ_B). So, as the reaction rate increases the oxygen coverage will rapidly fall to zero enabling the sensitive detection of the reducing gas.

1.1.3 *Parameters that Determine the Sensor Performance*

Sensitivity and selectivity are two important terms that determine a sensor's performance. Sensitivity is used to refer either the lowest concentration of a chemical species that can be detected or the smallest concentration increment that can be detected, and is usually designated by the sensor's resistance or the current passing through the sensor in the analyte over the sensor's resistance or the current passing through the sensor in air. Selectivity refers to the ratio of the sensor's ability to detect what is of interest over the ability to detect what is not of interest [19]. Figure (1.3) shows the equivalent circuit for a SnO_2 gas sensor [11]. Therefore, any effect that causes a change in the surface, bulk, contact or grain boundary properties will also change the sensor performance. There are many ways to change the electrical properties of these equivalent circuit elements such as; changing the geometry or form of the sensor and/or contacts (e.g. thick films, thin films), changing the microstructure (e.g. grain size, porosity), use of temperature control, use of catalysts and promoters, use of specific surface additives, and use of filters.

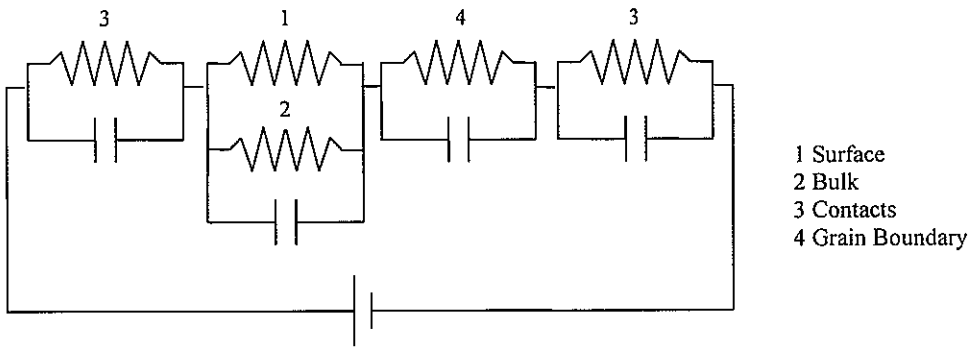

Figure 1.3: Schematic representation of the equivalent circuit for SnO_2 (taken from Gopel and Schierbaum [11]).

By making thick or thin films or by increasing the porosity the surface area will be increased. Consequently, the adsorption kinetics will be enhanced. In addition, the response time of the sensor will decrease since the material will equilibriate with the atmosphere in less time.

The rate of adsorption and the reaction between the adsorbed species depends, of course, on temperature. Sensitivity vs. temperature curves of semiconductor gas sensors usually shows a maximum at certain temperature which is used as the working temperature of that sensor. In addition to the effect of temperature on the kinetics of the reaction between the adsorbed species, findings on ZnO sensors reveal another effect of temperature on sensing. It was observed that, as the temperature was changed, the form of the adsorbed oxygen was also changed [20]. Therefore, the generally observed shape of the sensitivity curve is also affected by the changes in the nature and coverage of adsorbed oxygen as a function of temperature. This temperature which shows the maximum sensitivity can be used as a means of selectivity between reducing gases having maxima at different temperatures.

If a surface additive that specifically adsorbs or reacts with the gas of interest is used, then this can increase selectivity. Use of hygroscopic salts for humidity sensors and use of sulfanilic acid for NO_2 sensing are the examples of this technique. Using filter materials is another technique in which a coating is used to either consume the gases which are not of interest or permit the passage of the gas which is of interest. For example, platinum and palladium are known to facilitate the hydrogen gas diffusion [21], and zirconia can be used at high temperatures to facilitate oxygen diffusion [22]. Zeolites are also used as filters since they adsorb many gases [23].

Catalysts enhance both the response time and selectivity in gas sensors. Platinum and palladium are the most popular of these [24], which induce spillover of hydrogen atoms. In this process, the metal catalyst dissociates the gas molecule, and then the atoms can spillover onto the surface of the semiconductor. The bonding energy of the hydrogen atoms to platinum is close to the bonding energy of the hydrogen atoms to each other, so it requires very little energy to dissociate the hydrogen in this way. Similarly, the oxygen atoms are also dissociated on the platinum. On the other hand, without the catalyst, a very high amount of energy is required in order to dissociate the gas molecules into their substituent atoms. Although this energy is recovered when the hydrogen and the oxygen atoms react to form H_2O, the large dissociation energy required presents a large activation energy. Moreover, the bonds between platinum and hydrogen, and the bonds between platinum and oxygen are relatively unstable, so the H and O are highly activated.

For these processes to dominate the sensor resistance, the spilled-over species must be able to migrate to the intergranular contact. Thus, for a catalyst to be effective, one must have a good dispersion of the catalyst particles, so that they can be available near all intergranular contacts.

Promoters are surface additives that are not catalysts but they can enhance the selectivity or reactivity of the catalyst. They can do this in several ways such as [25]; stabilizing a valence state or stoichiometry, favoring the promotion of active phases, and increasing the electron exchange rate. They can also change the sensitivity of the sensor and the temperature at which the maximum sensitivity is observed [26].

1.1.4 *Smart Gas Sensors*

Conventional semiconductor gas sensors have been used for more than 30 years. A chemical sensor should possess characteristics such as selectivity, sensitivity, reproducibility, and stability. However, these materials still present problems to be solved, such as insufficient gas selectivity, and inability to detect very low gas concentrations [27]. Recently, Yanagida proposed searching for intelligent mechanisms instead of trying to optimize existing compositions, processes or integration techniques [28]. He has defined intelligent ceramics as the ceramic materials which have properties such as self diagnosis, self recovery, self adjustment, stand by and tuning ability from outside. Systems having these properties, the properties of a living organ, can be used under very harsh and hazardous environments that living organisms cannot survive. The heterocontact sensor made by a *p-n* contact between *p*-type CuO and *n*-type ZnO is a very good example of such an intelligent mechanism. These sensors can be used as humidity sensors with a self recovery mechanism or as gas sensors in which selectivity towards a certain gaseous species can be tuned.

1.2 Heterocontact Gas Sensors

1.2.1 *p-n Junctions*

p-n junctions are fabricated by forming a contact between a *p*-type and an *n*-type semiconductor. The junction shows rectifying properties in that a current in one direction can flow quite easily whereas in the other direction it is limited by a leakage current which is generally very small. The basic theory of current-voltage characteristics of *p-n* junctions was established by William Shockley in his explanations of the transistor operation [29].

1.2.1.1 *No Applied Bias*

Consider one side of a Si sample is *p*-type doped and the other side is *n*-type doped as shown in Figure (1.4) [30]. We assume there is an abrupt junction in which the impurity concentration in the semiconductor changes abruptly from acceptor impurities to donor impurities which is called the metallurgical junction.

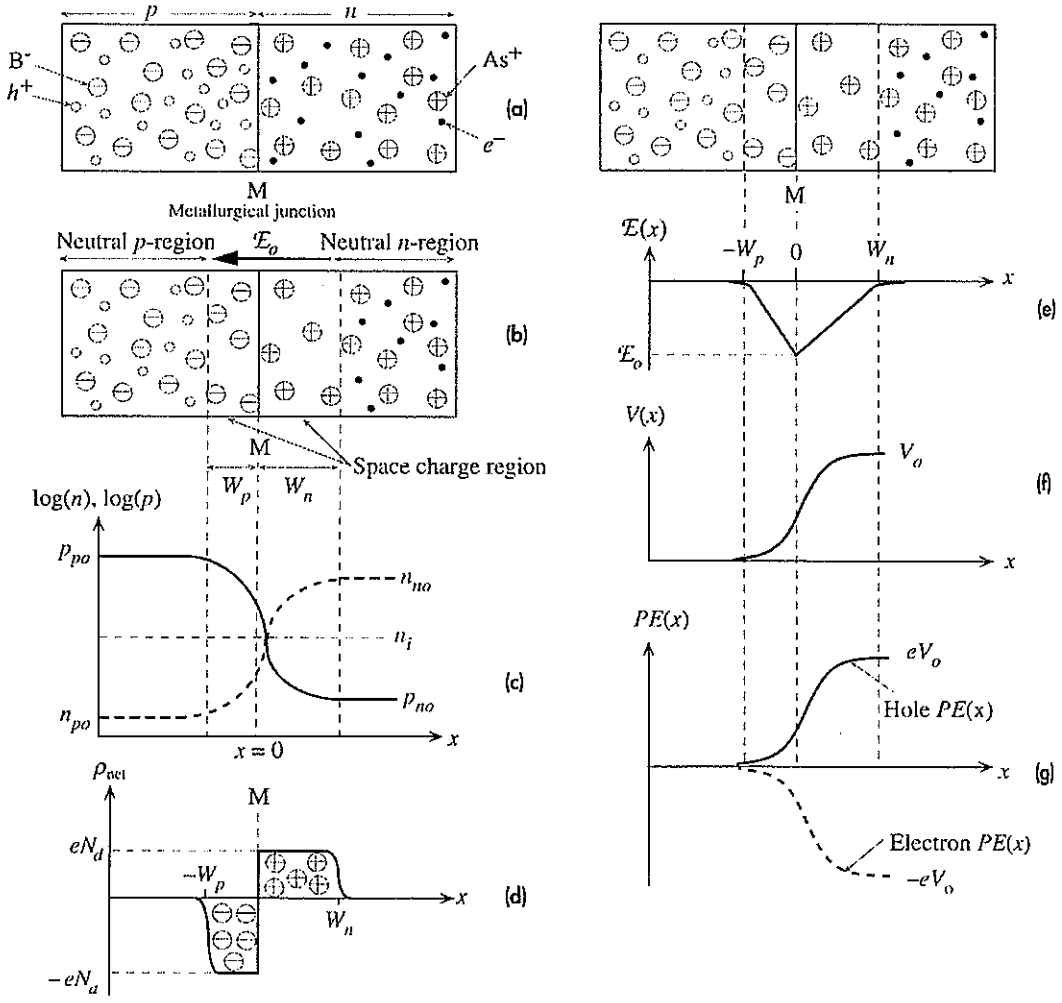

Figure 1.4: Properties of the *p-n* junction (taken from Kasap [30]).

Due to the concentration gradient the holes diffuse from the *p*-side to the *n*-side. Similarly, electrons diffuse from the *n*-side to the *p*-side. Holes diffusing through the *n*-side (Figure 1.4a right) recombine with the electrons in the *n*-side near the junction. Similarly, electrons diffusing through the *p*-side (Figure 1.4a left) recombine with the holes in the *p*-side near the junction. Consequently, there is a region depleted of charge carriers form near the junction. It is important to note that when there is no applied bias the condition $pn = n_i^2$ is valid everywhere. The depletion region is also called a space charge layer since the recombined charge carriers leave behind donor (N_d) or acceptor (N_a) ions. In this region, an electric field is built from positive ions to negative ions, which acts to drift holes back into the *p*-side and electrons back into the *n*-side. As more holes diffuse toward the right, and more electrons toward the left, the electric field will increase until an equilibrium is reached where the rate of diffusing holes toward the right is equal to the rate of holes drifting to the left by the electric field. The electron diffusion and drift will also be balanced. For uniformly doped *p*- and *n*-regions the net space charge density across the space charge layer will be as shown in Figure (1.4d). Defining $W = W_n + W_p$ as the space charge width, it will be $-eN_a$ from $x = -W_p$ to 0, and eN_d from $x = 0$ to W_n. The total charge on the left should be equal to that on the right, that is

$$N_a W_p = N_d W_n \tag{1.11}$$

In the Figure we assumed that $N_d < N_a$. From Equation (1.11), this implies that $W_n > W_p$, which means the depletion region penetrates more to the *n*-side than it does to the *p*-side.

The electric field is related to the net space charge density by the equation:

$$E(x) = \frac{1}{\varepsilon} \int_{-W_p}^{x} \rho_{net}(x)dx \tag{1.12}$$

where ε is the permittivity of the medium. The variation of electric field across the junction is shown in Figure (1.4e). The negative sign shows its direction and E(x) reaches a minimum, E_o, at the metallurgical junction. The potential V(x) at any point can be found by integrating E = -dV/dx. Figure (1.4f) shows the potential change across the junction, and the potential at x = $-W_p$ is taken as 0, which is an arbitrary reference level. Since we considered an abrupt junction, we can describe ρ_{net} by step functions, and we can write E_o by integrating Equation (1.12) as:

$$E_o = -\frac{eN_d W_n}{\varepsilon} = -\frac{eN_a W_p}{\varepsilon} \tag{1.13}$$

And then derive V_o, built-in voltage, which is the potential at x = W_n as:

$$V_o = -\frac{1}{2} E_o W_o = \frac{eN_a N_d W_o^2}{2\varepsilon(N_a + N_d)} \tag{1.14}$$

where $W_o = W_n + W_p$ is the depletion region width. The built-in voltage can be related to the doping parameters via Boltzmann statistics:

$$\frac{n_{po}}{n_{no}} = \exp\left(-\frac{eV_o}{k_B T}\right) \tag{1.15}$$

Once we know the built-in voltage we can calculate the depletion region width from Equation (1.14) as:

$$W_o = \left[\frac{2\varepsilon(N_a + N_d)V_o}{eN_a N_d}\right]^{\frac{1}{2}} \tag{1.16}$$

1.2.1.2 *Forward and Reverse Biases*

When a battery is connected to the *p-n* junction so that the positive terminal of the battery is attached to the *p*-side and the negative terminal is attached to the *n*-side, and if the

applied voltage is V, then the potential barrier V_o will be reduce56d by V, as shown in Figure (1.5). This drop in potential will allow many holes to diffuse across the depletion region and entering the *n*-side, which results in the injection of excess minority carriers, holes, into the *n*-side. Similarly, the electrons can easily diffuse toward *p*-side and become injected minority carriers.

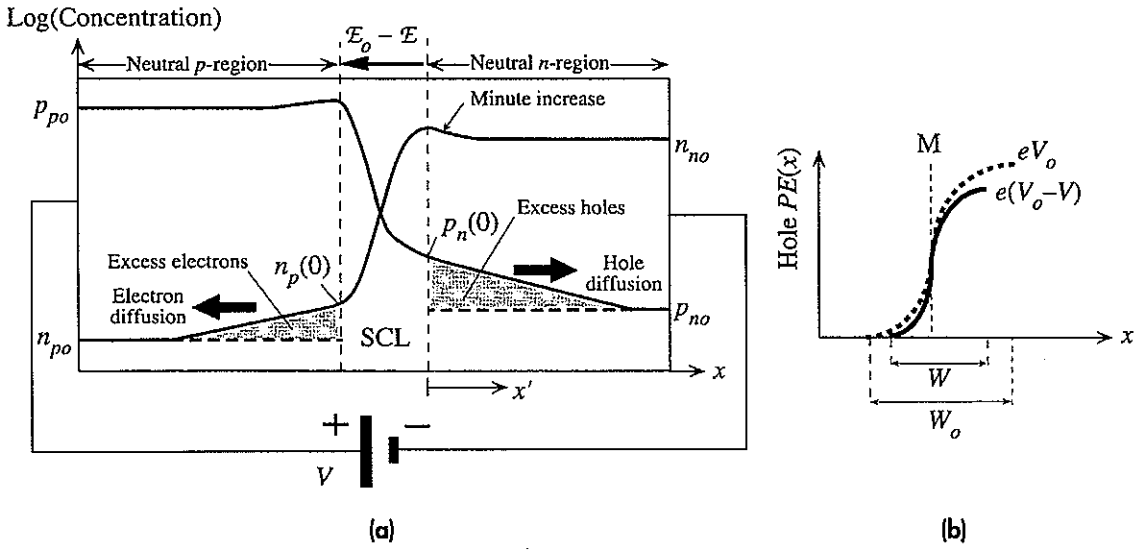

Figure 1.5: Forward biased *p-n* junction and the injection of minority carriers (taken from Kasap [30]).

The hole concentration just outside the depletion region in the *n*-side, and the electron concentration just outside the depletion region in the *p*-side can be calculated using Boltzmann statistics as:

$$p_n(0) = p_{no}\exp\left(\frac{eV}{k_BT}\right) \qquad \text{and} \qquad n_p(0) = n_{po}\exp\left(\frac{eV}{k_BT}\right) \tag{1.17}$$

which is called the law of junction.

The holes diffused into *n*-side will recombine with the electrons in this region. Those electrons lost by the recombination will be replenished by the negative terminal of the battery connected to this side. The current due to holes diffusing into *n*-region can be sustained because more holes can be supplied by the *p*-region, which itself can be replenished by the positive terminal of the battery. Similarly, in the *p*-side injected electrons will recombine with the holes in this region. Those holes lost by the recombination will be replenished by the positive terminal of the battery connected to this side. The current due to electrons diffusing into *p*-region can be sustained because more electrons can be supplied by the *n*-region, which itself can be replenished by the negative terminal of the battery. Consequently, an electric current will be maintained through the *p*-*n* junction due to the diffusion of minority carriers. Drift of majority carriers will also have some effect.

Some of the minority carriers will also recombine in the depletion region. Consequently, there will be a current due to this recombination. Therefore, the total diode current will be the sum of the diffusion current and the recombination current. The current can be expressed as:

$$I = I_o\left[\exp\left(\frac{eV}{\eta k_B T}\right) - 1\right] \tag{1.18}$$

where η is an ideality factor, which is 1 when the current is due to diffusion and 2 when it is due to recombination.

When the junction is reverse biased, the built-in potential barrier will increase as shown in Figure (1.6). The negative terminal of the battery will attract holes in the *p*-side to move away from the space charge layer, which results in more negative acceptor ions, and hence a wider space charge layer. Similarly, the positive terminal will attract electrons away from the space charge layer. The movement of electrons toward the positive terminal of the battery cannot be sustained because there is no electron supply to the *n*-side. The *p*-side cannot supply electrons to the *n*-side because it has hardly any. However, there is a small reverse current due to two causes.

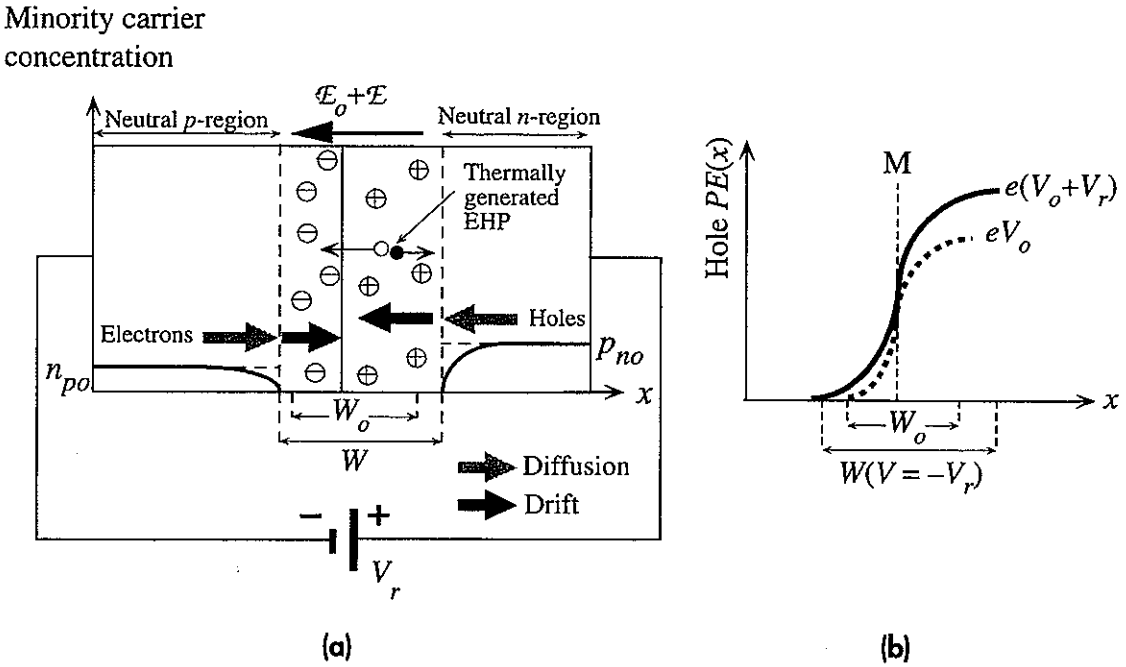

Figure 1.6: Reverse-biased *p-n* junction (taken from Kasap [30]).

The hole concentration just outside the space charge layer in the *n*-side is nearly zero, whereas the hole concentration in the bulk, p_{no}, is very small. This small concentration gradient causes a small hole diffusion current toward the space charge layer. Similarly, there

is a small electron diffusion current from *p*-side toward the space charge layer. Within the space charge layer, these carriers are drifted by the field. This minority carrier diffusion current is the Shockley model.

The other cause for the small reverse current is the thermal generation of electron-hole pairs (Figure 1.7). As shown in Figure (1.6), the internal field in the space charge layer will separate the electron and the hole and drift them toward the neutral regions. Minority carrier diffusion depends on the material and the temperature but not on the voltage. The current due to space charge layer generation depends also on the voltage (Figure 1.7).

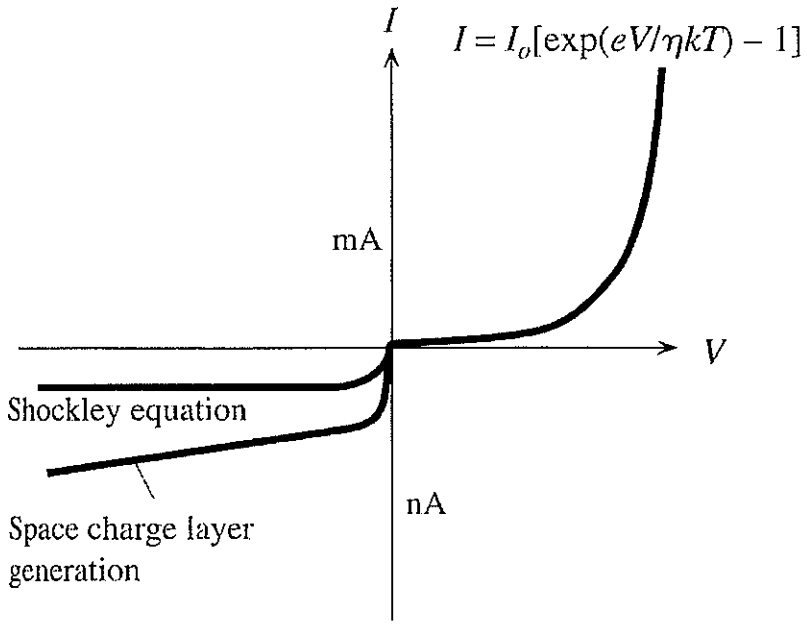

Figure 1.7: Forward and reverse I-V characteristics of a *p-n* junction (taken from Kasap [30]).

1.2.1.3 *p-n Junction Band Diagrams*

Figure (1.8) shows the *p*-type and *n*-type semiconductors of the same material before contact and when they are in contact. In the figure, the work function of the semiconductors (Φ_p, Φ_n), the Fermi levels (E_{Fp}, E_{Fn}), and the energy gaps, E_g between the conduction and the valence bands are also shown. When the two semiconductors are brought into contact, in equilibrium E_F must be uniform through the two materials (otherwise work is done by the system or on the system). The electrons will diffuse from the *n*-side to the *p*-side and deplete the *n*-side near the junction. Similarly, the holes will diffuse from the *p*-side to the *n*-side and deplete the *p*-side near junction. Furthermore, diffusing holes and electrons will recombine and form a depletion region or a space charge layer in the vicinity of the junction.

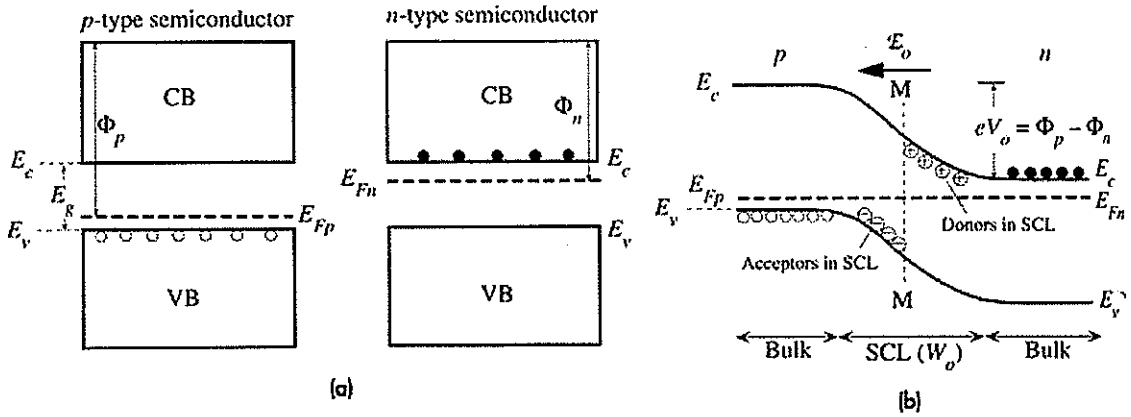

Figure 1.8: (a) Two isolated *p*- and *n*-type semiconductors (same material), (b) band diagram after contact (taken from Kasap [30]).

In the region which is depleted of holes, E_v will move away from E_{Fp} and similarly, in the region which is depleted of electrons, E_c will move away from E_{Fn}. Therefore, band bending will be observed. Band bending will also account for the observed built-in potential (or the

built-in field). In the space charge region the Fermi level will not be close to E_c or E_v, since this region is depleted of charge carriers.

Figure (1.9) shows the band diagrams for the *p-n* junction under different bias conditions. When there is a forward bias, the potential barrier is reduced by the amount of the

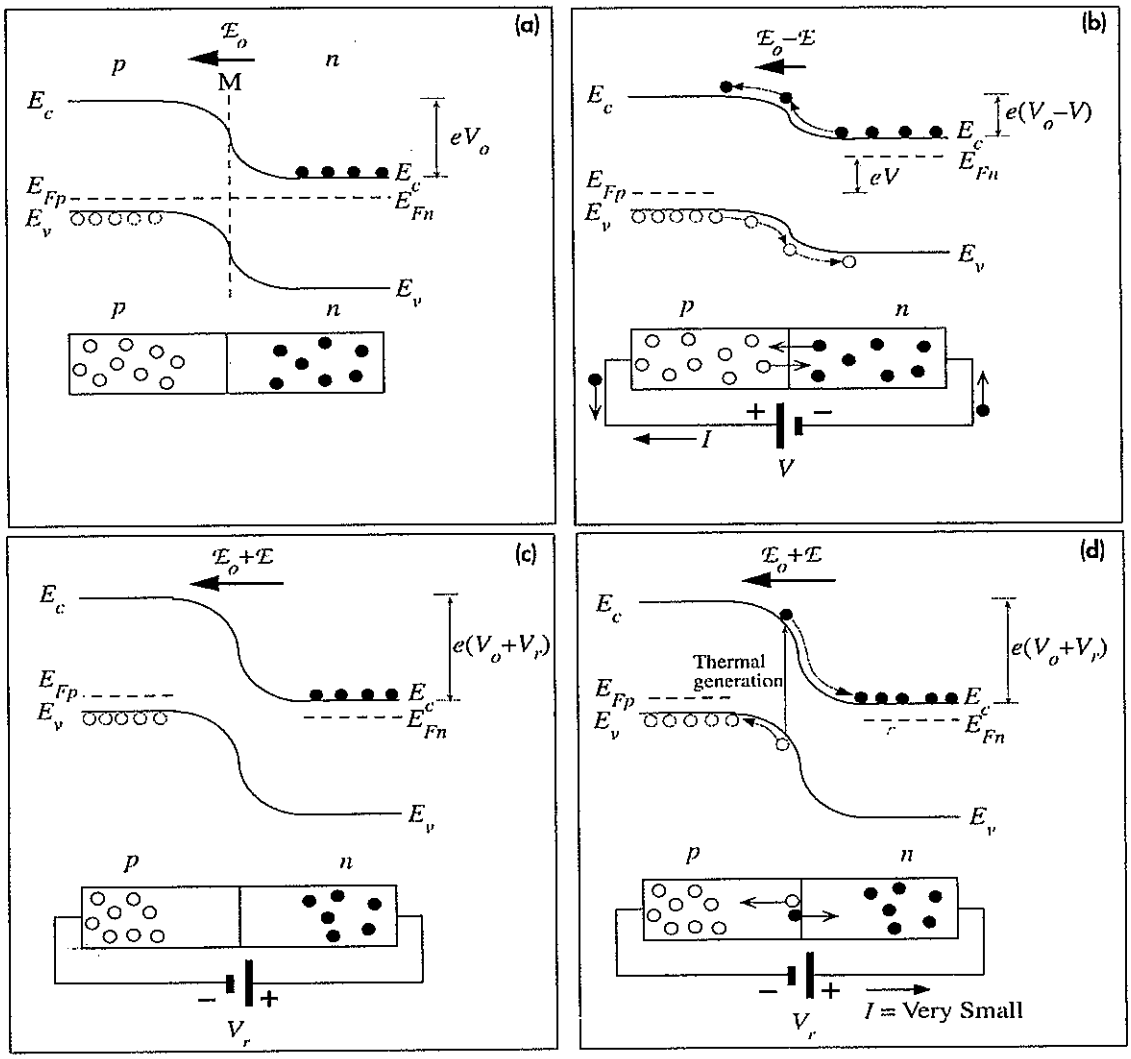

Figure 1.9: Energy band diagrams for a *p-n* junction (a) open circuit, (b) forward bias, (c) reverse bias conditions, (d) thermal generation of electron-hole pairs (taken from Kasap [30]).

applied voltage, and since the diffusing charge carriers are replenished by the terminals of the battery, there is a current flowing through the junction and around the circuit. There is still a drift current due to electrons being drifted by the electric filed within the space charge region.

When there is a reverse bias, the potential barrier is increased by the applied voltage. The diffusion current is negligible (since the charge carriers cannot be replenished by the terminals of the battery), and there is a very small current due to thermal generation of electron-hole pairs.

1.2.1.4 *Depletion Layer Capacitance*

The depletion region of the *p-n* junction has separated positive and negative charges over a distance (depletion layer width), similar to a parallel plate capacitor. However, the stored charge in the depletion region does not depend linearly on the voltage like a parallel plate capacitor. The depletion layer capacitance is defined by:

$$C_{dep} = \left| \frac{dQ}{dV} \right| \tag{1.19}$$

where the amount of charge in the depletion layer is, $|Q| = eN_d W_n A = eN_a W_p A$, and A is the cross-sectional area. Differentiating Equation (1.19) and substituting Equation (1.17) we get:

$$C_{dep} = \frac{\varepsilon A}{W} = \frac{A}{(V_0 - V)^{\frac{1}{2}}} \left[\frac{e\varepsilon(N_a N_d)}{2(N_a + N_d)} \right]^{\frac{1}{2}} \tag{1.20}$$

The depletion layer capacitance is present under both forward and reverse bias conditions.

1.2.1.5 *Reverse Breakdown (Avalanche and Zener Breakdown)*

As the reverse bias increases, drifting electrons in the space charge layer gain sufficient energy to ionize host crystal atoms by bombardment, which is called impact

ionization. A new electron-hole pair is generated by the process. The electron-hole pairs generated by impact ionization themselves can be accelerated by the electric field and give rise to new electron-hole pairs and so on, leading to an avalanche effect.

Heavily doped *p-n* junctions have narrow depletion widths, as shown in Figure (1.10). Zener breakdown is the enormous increase in the reverse current in a *p-n* junction when the applied voltage is sufficient to cause the tunneling of electrons from the valence band in the *p*-side to the conduction band in the *n*-side.

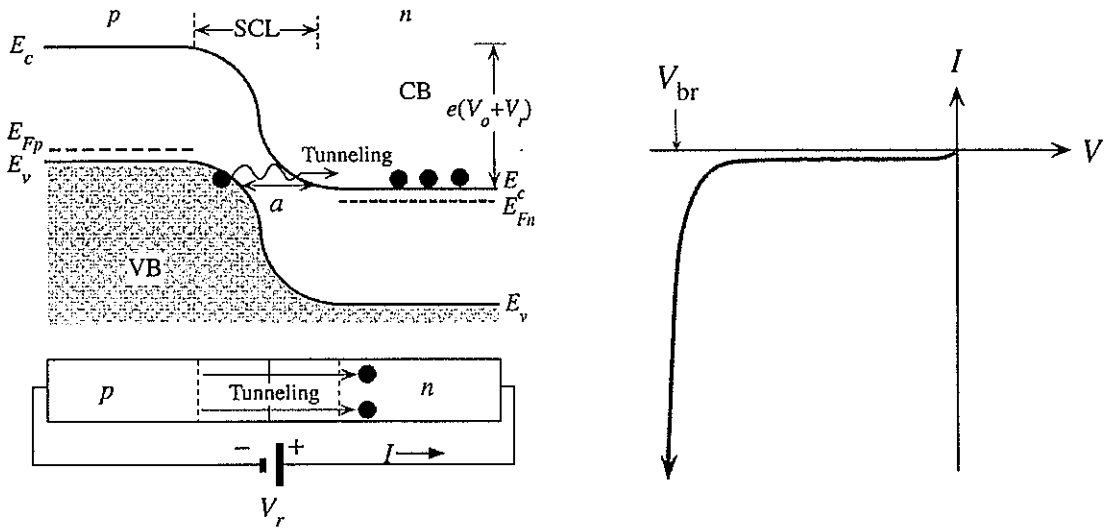

Figure 1.10: Zener breakdown and reverse I-V characteristics of a *p-n* junction (taken from Kasap [30]).

1.2.2 *p-n Heterojunctions*

Heterojunctions are *p-n* junctions formed between dissimilar materials. The electronic behavior of heterojunctions is similar to that of homojunctions except for new boundary conditions at the interface. The transition between two materials at the interface causes a discontinuity in the conduction band edges (ΔE_c) and valence band edges (ΔE_v). These

discontinuities originate from band offsets, carrier effective mass, carrier mobility and the dielectric constant difference between the two materials [31, 32]. Figure 1.11 shows the energy-band diagram of a heterojunction formed between a narrow gap *p*-type semiconductor (e.g. CuO) and a wide gap *n*-type semiconductor (e.g. ZnO). The materials also have different dielectric constants (ε), different work functions (Φ), and different electron affinities (χ). In the following case, since the narrow gap material has a larger work function, the energy bands of the *p*-side will be bent downwards and the energy bands of the *n*-side will be bent upwards. The band discontinuities may be expressed as [32]:

$$\Delta E_c = E_{c1} - E_{c2} - eV_0 \quad \text{and} \quad \Delta E_v = E_{g1} - E_{g2} - \Delta E_c \tag{1.21}$$

where E_{c1} and E_{c2} are the edges of conduction bands of the two materials, E_{g1} and E_{g2} are the band gaps, and V_o is the built-in potential.

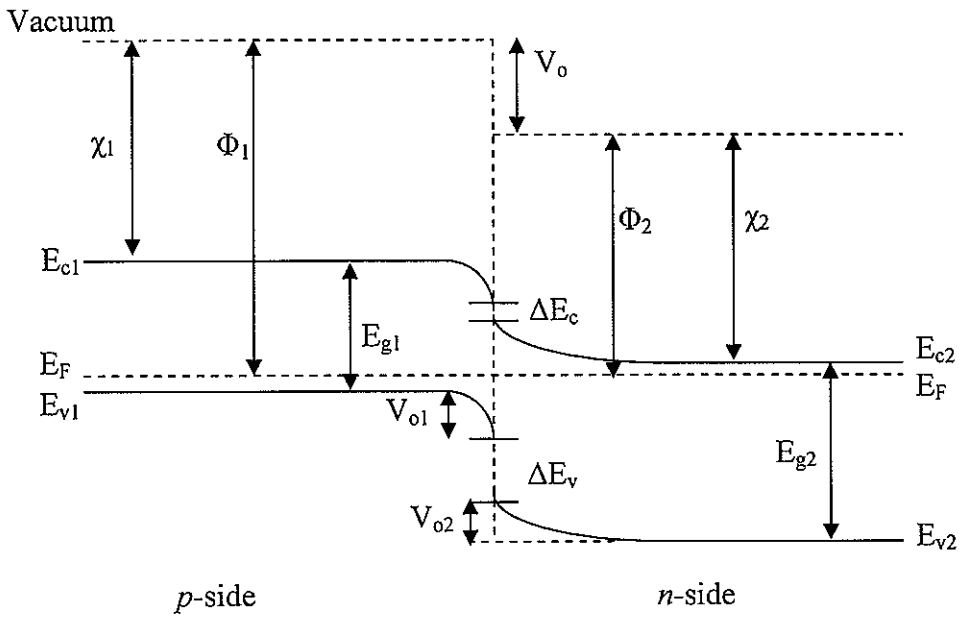

Figure 1.11: Energy-band diagram of *p-n* Heterojunction.

The discontinuities in the band edges at the interface results in different barrier heights for the two types of carriers, and hence the current through the heterojunction in most cases consists almost entirely of either electrons or holes. The variation of the current with applied voltage for a heterojunction is given by [31]:

$$I = A\exp\left(-\frac{eV_{B2}}{k_BT}\right) - B\exp\left(-\frac{eV_{B1}}{k_BT}\right) \tag{1.22}$$

where V_{B1} is the barrier that carriers in semiconductor 1 must overcome, and V_{B2} is the barrier for the carriers moving in the opposite direction. The coefficients A and B depend on doping levels, carrier effective mass, and the specific transport mechanism. For the junction shown in Figure 1.11 the barrier for electrons is smaller than that for holes, therefore the current will be dominated by the electrons and V_{B2} will exist for the predominant carrier. The variation of current will then be given by:

$$I = A\exp\left[-\frac{eV_{D2}}{k_BT}\right]\left[\exp\left(\frac{eV_2}{k_BT}\right) - \exp\left(-\frac{eV_1}{k_BT}\right)\right] \tag{1.23}$$

where V_1 and V_2 are the portions of applied voltage appearing in materials 1 and 2 and V_{o1} and V_{o2} are the potentials supported at equilibrium by materials 1 and 2, respectively. The first term in the brackets is important for forward bias and the second for reverse bias.

1.2.3 *Use of p-n Heterojunctions as Gas Sensors*

The use of heterocontact as gas sensors was first proposed by Yanagida *et al.* in 1986 [33]. The sensor was simply made by mechanically contacting a *p*-type CuO ceramic and an *n*-type ZnO ceramic pellet. The sensor was called a heterocontact instead of a heterojunction, since it has a large amount of non-contacting area which is exposed to the surrounding atmosphere. The heterocontact showed a high sensitivity and selectivity to CO gas over H_2,

which has been a problem for SnO_2 or other semiconductor gas sensors since their working mechanism is based on the catalytic oxidation of gas molecules. H_2 undergoes facile oxidation on many *n*-type semiconductor surfaces, and hence these are typically more sensitive to H_2 than CO.

The working mechanism that Yanagida *et al.* suggested was that the adsorbed molecules of reducing gases form interface states that can change the potential barrier height and consequently the current across the junction. Later, they proposed a model for CO oxidation at the interface of CuO and ZnO as follows [34]: (i) CO and O_2 gas molecules adsorb preferentially on CuO and ZnO, respectively; (ii) due to chemisorption, charge transfer from the ceramic to the adsorbed gases takes place; holes are transferred to CO, and electrons are transferred to O; (iii) CO^+ on the CuO surface, and O^- on the ZnO surface react to form CO_2 molecules; (iv) the CO_2 molecules generated through this process are then desorbed from the interface leaving behind sites for the adsorption of new gas molecules. This model is schematically shown in Figure (1.12).

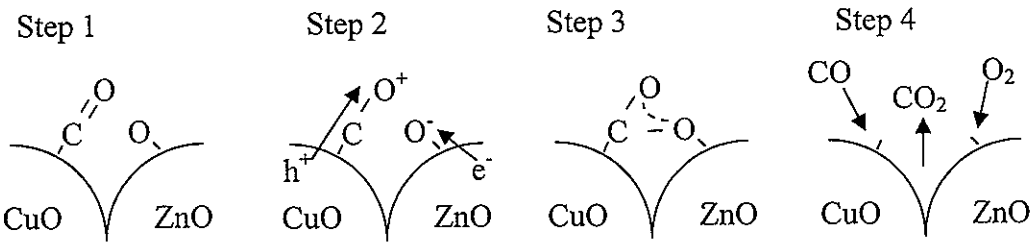

Figure 1.12: The model proposed by Yanagida *et al* (taken from Yanagida *et al.* [32]).

The reaction scheme can be written as:

$$O_2 + 2e^- \rightarrow 2O^- \quad [ZnO] \tag{1.24}$$

$$CO + h^+ \rightarrow CO^+ \quad [CuO] \tag{1.25}$$

$$CO^+ + O^- \rightarrow CO_2 \quad [\text{interface}] \tag{1.26}$$

Reaction (1.26) corresponds to the carrier recombination at the interface of the *p-n* junction which decreases the potential barrier height, thus enabling the detection of CO. However, carbon monoxide will react with oxygen both on the interface of the heterocontact and on the surface of CuO. Therefore, reaction (1.26) should be enhanced, instead of increasing the catalytic reaction of adsorbed carbon monoxide and oxygen on the surface of CuO. This is shown by the addition of the alkali metal Na to CuO [35]. The addition of electropositive alkali metal ion stabilized the chemisorption reaction and promoted the adsorption of CO and O_2 [36]. It was also suggested that the presence of extra holes introduced by Na promoted a strong adsorption of CO gas [37]. So, stable and long-lifetime CO adsorbates on Na doped CuO enhanced reaction (1.26) and consequently, adsorbed oxygen on ZnO was consumed efficiently. On the other hand, for the heterocontact with pure CuO, much less sensitivity is observed, since pure CuO is more catalytic than Na doped CuO and CO adsorbates have less chance of reacting with O^- on ZnO.

These studies give an insight into the sensing mechanism of CuO/ZnO heterocontact; however a rigorous model has not been definitely established yet. The interface states have been shown to play an important role on gas sensing properties of the heterocontact. Using equation (1.20), the built-in (or diffusion) potential V_o, can be obtained by plotting $1/C^2$ vs. V. The experimental values for the diffusion potential were found to be larger than the calculated values [38, 39]. This indicates that in addition to the depletion layer capacitance there is an interface-state capacitance, originating from the interface states which derive from chemical adsorbates, leading to the high diffusion potential.

The gas sensing and the density of interface states were shown to be dependent on the starting materials and the processing conditions [36, 38, 39]. Heterocontacts made by quenched (in air) CuO showed higher sensitivity to CO, and this was explained by the larger amounts of CO molecules with longer life-time on the surface of the quenched sample [40]. Hydrogen sensitivity was enhanced by making the heterocontact from porous ceramics [41]. The reproducibility and the integrity of the system was enhanced by preparing thin film heterocontacts [39, 42]. It is important to note here that even though the heterocontacts have been prepared in a very primitive manner relying on a mechanical contact, they exhibit well-defined rectifying characteristics, and high sensitivity to reducing gases.

The heterocontact sensor is unique in that its selectivity to a certain gaseous species can be tuned by changing the applied bias [43, 44]. Sensing properties can be tuned to detect

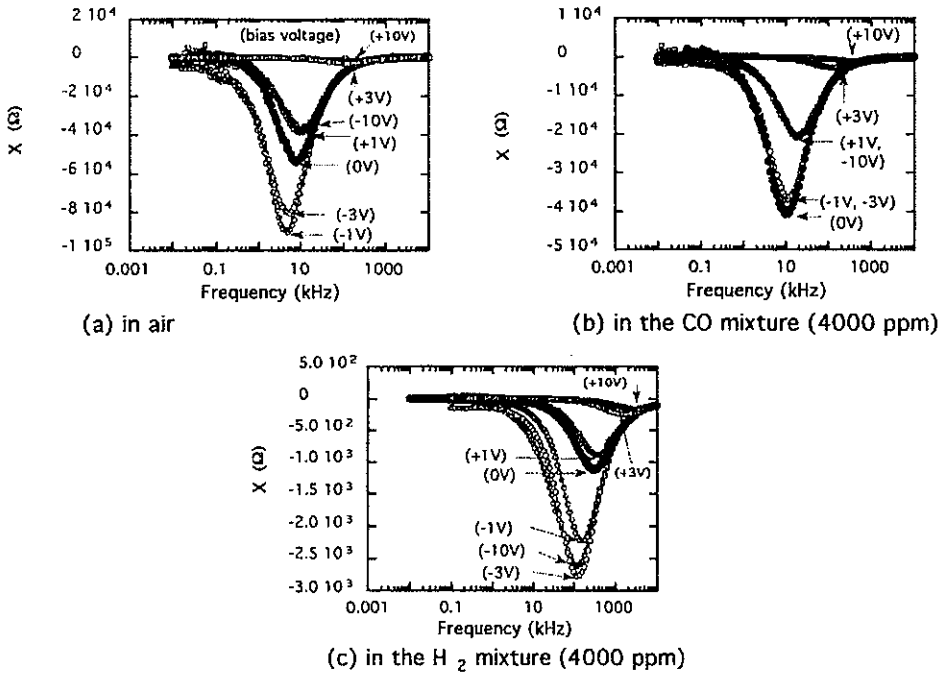

Figure 1.13: Dependence of reactance on frequency and applied dc bias (taken from Hikita, Miyayama, and Yanagida [42]).

CO and/or H_2 gases in air, by selecting the measuring frequency and the applied dc bias using an impedance analyzer. This can be achieved in number of ways. Figure (1.13), shows the frequency dependence of reactance of the heterocontact sensor. As the bias is changed from 0 V to -10 V, the value of the minimum peak of the reactance increases in air and in CO, whereas in H_2 it decreases. The bias dependence of normalized reactance (normalized by the reactance under bias of 0 V in each testing gas) can also be used for selecting between gases, as shown in Figure (1.14). The gases exhibit opposite signs for reactance change when the dc bias moves from 0 V to the negative range. Another way is to use the frequency dependence of reactance. As depicted in Figure (1.15), both gases can be detected with a low frequency measurement; H_2 can be detected at high frequencies; and CO can be detected if reactance changes at both high and low frequencies are analyzed.

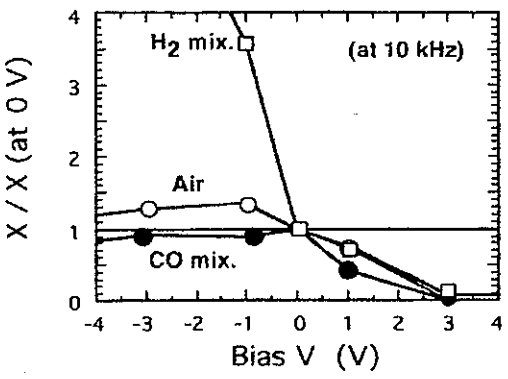

Figure 1.14: dc bias dependence of reactance at 10 kHz, 400 °C (taken from Hikita, Miyayama, and Yanagida [42]).

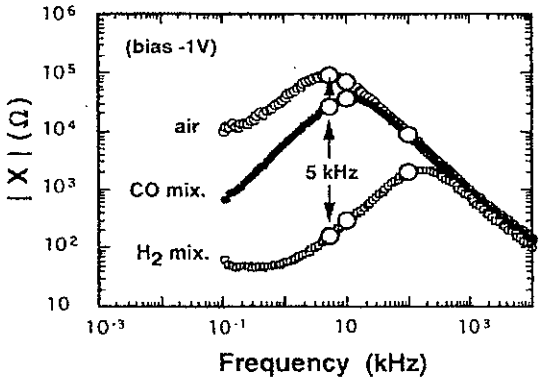

Figure 1.15: ac frequency of absolute value of reactance under dc bias of -1 V (taken from Hikita, Miyayama, and Yanagida [42]).

The tunable sensing property can be evaluated through an equivalent circuit for the heterocontact in a reducing atmosphere, shown in Figure (1.16) [45]. Here R_s is the bulk resistance, R_i and C_i are interface resistance and capacitance respectively, R_{io} and C_{io} denotes the air atmosphere, and R_{ads} and C_{ads} are derived from the adsorption or reaction of reducing gases. The resistance and the capacitance at the interface can be written as [44]:

$$C_i = C_{io} + C_{ads} = \mathbf{a}C_{io} \tag{1.27}$$

$$R_i = \left(R_{io}.R_{ads}\right)/\left(R_{io} + R_{ads}\right) = \mathbf{b}R_{io} \tag{1.28}$$

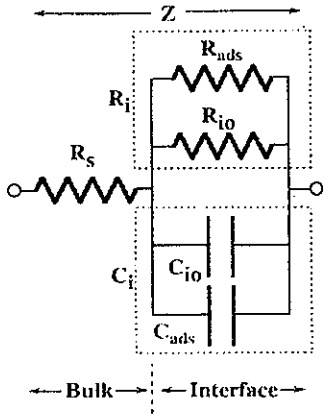

Figure 1.16: Equivalent circuit of heterocontact with additional circuit elements in a reducing gas atmosphere (taken from Miyayama *et al.* [43]).

Assuming the bulk resistance R_s is negligible, reactances X_o (in air) and X (in a reducing atmosphere) are written as:

$$X_o = \omega C_{io} R_{io}^2 / \left(1 + \omega^2 C_{io}^2 R_{io}^2\right) \tag{1.29}$$

$$X = -\omega\left(\mathbf{a}\mathbf{b}^2\right) C_{io} R_{io}^2 / \left[1 + \omega^2 \left(\mathbf{a}^2\mathbf{b}^2\right) C_{io}^2 R_{io}^2\right] \tag{1.30}$$

The angular frequency, ω, at the minimum reactance in a reducing atmosphere is given by, $dX/d\omega = 0$, as

$$\omega = 1/(C_i R_i) = 1/[(\mathbf{a}C_{io})(\mathbf{b}R_{io})] = (\omega_o / \mathbf{ab}) \tag{1.31}$$

where ω_o is the angular velocity at the minimum reactance in air. According to Equation (1.31), the frequency producing the minimum reactance is inversely proportional with the product C_iR_i. When C_iR_i approaches **ab** = 1, the angular frequency, ω approaches ω_o, which equals the value in air. If the introduction of the reducing gases can change the capacitance, C_i, and the resistance, R_i, to give **ab** < 1 or **ab** > 1, the absolute value and the frequency dependence of the reactance should change. Furthermore, if **ab** changes with the applied bias, the frequency producing the minimum reactance should also change with the bias. Evaluation of **ab** can be done by comparing C_iR_i in air and in reducing gases. For gas identification, the product C_iR_i must have different dependencies on frequency and on applied bias in each gas atmosphere.

The catalytic reaction of the reducing gases was shown to be enhanced when the reverse bias was applied [44, 46, 47]. The working mechanism of this phenomenon for CO gas was discussed by Wolkenstein's electronic theory of catalysts [48]. Yanagida *et al.* proposed a model showing the relation between the catalytic activity and the Fermi level position of a catalyst. They supposed that the oxidation of CO over CuO proceeds by the Rideal mechanism and expressed the reaction rate as [47]:

$$r = \alpha N_o \eta_o^- P_{CO} \tag{1.32}$$

where α is a constant, η_o^- is the occupancy of a negative charge on the adsorbed species, N_o is the amount of adsorbed oxygen and P_{CO} is the partial pressure of CO. The relation between the surface Fermi level position, ε_s^+, and η_o^- is illustrated in Figure (1.17).

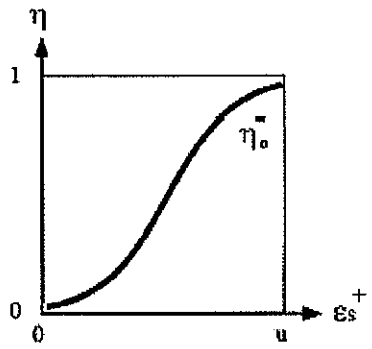

Figure 1.17: The relation between the surface Fermi level position, ε_s^+, and the occupancy of a negative charge on chemical species η_o^- (taken from Nakamura *et al.* [45]).

When the surface Fermi level is raised up the value of η_o^- increases and as a result the reaction rate increases. If the p-i-n (semiconductor-insulator-semiconductor) model is assumed at the interface, the surface Fermi level of CuO would be raised up by applying reverse bias and the amount of O^- will be increased. Consequently, the catalytic activity of the CuO surface would be enhanced.

Heterocontact systems other than CuO/ZnO have also been studied for gas sensing. Different *p-n* materials have been used such as La_2CuO_4/ZnO, $LnMO_3/SnO_2$, Ln_2CuO_4/SnO_2 (Ln = rare earth, M = Cr, Co, Mn, Fe) [27, 49-52]. Among these systems La_2CuO_4/ZnO showed well defined rectifying characteristics, and a high sensitivity to reducing gases, especially to H_2 gas.

CHAPTER 2. EXPERIMENTAL PROCEDURES

2.1 Material Preparation

Polycrystalline samples of CuO and ZnO were synthesized via solid state methods. The batches were prepared using appropriate stoichiometric amounts of powders of ZnO (Aldrich, 99+%), CuO (Alfa Aesar, ACS), Li_2CO_3 (Aldrich 99+% ACS), Na_2CO_3, $CaCO_3$ (Fisher, ACS), $SrCO_3$ (99+%), Ga_2O_3 (All-Chemie, 99.999%), and NiO (Alfa Aesar 99%). After that, the powders were milled in zirconia media for 6 h and then dried overnight. Doped CuO powders were calcined at 800 °C and doped ZnO powders were calcined at 900 °C for 12 h in air. After re-milling and drying the powders, 1 wt % PVA (poly vinyl alcohol) binder was added to powders to aid sintering. The CuO and ZnO pellets were then pressed into 12.7 mm diameter pellets by cold uniaxial pressing under pressure of 100 MPa and 20 MPa, respectively. For binder burn-out, the pellets were heated up to 500 °C with a rate of 1 °C/min and held at that temperature for 3h. Then, they were heated up to their sintering temperatures with a rate of 5 °C/min. The CuO pellets were sintered at 900 °C for 24 h, and ZnO pellets were sintered at 1000 °C for 3 h using a Carbolite high temperature tube furnace in flowing air. Densities of the pellets were calculated using the Archimedes method. The pellets were polished using SiC emery paper (Grit 600/P1200) and parallel surfaces were obtained. The pellets were 1 mm in thickness. After washing the pellets with acetone, Heraeus (C1000) silver electrodes were painted on one side of the pellets and the pellets were fired at 550 °C for 30 mins.

2.2 Property Measurements

The electrical measurements of the *p-n* heterocontacts were made in a NorECs Probostat™ conductivity cell. The heterocontact was made by mechanically contacting CuO and ZnO pellets using the spring force of the cell. Figure (2.1) shows the experimental setup. The electrical properties of the samples were measured in dry air and in H_2 (4000 ppm). Dry air (N_2:O_2 = 4:1) was used as the carrier gas for H_2, and the concentration and flow rate of the gases were controlled by Aalborg gas mass flow controllers. The samples were equilibriated at the measuring temperature and atmosphere for 30 mins. The flow rate was fixed at 200 mL/min. A Keithley 237 high voltage source measure unit was used for dc current-voltage measurements with an applied bias ranging from -20 to +20 V at a step of 1 V. The current values were measured 1 s after a voltage is applied. Current-time measurements were conducted at 0.5 V in air/H_2 and air/N_2 atmospheres. For ac capacitance measurements an HP 4284A LCR meter was used. Impedance measurements were made by an HP 4194A impedance analyzer, at frequencies ranging from 100 Hz to 5 MHz under a dc bias voltage (-10 to +10 V) with the application of an ac signal (oscillation voltage of 0.5 V) in controlled gas atmosphere at 400 °C.

In impedance spectroscopy, ac impedance measurements are made over a wide range of frequencies and the different regions of the material are characterized according to their electrical relaxation times or time constants. Impedance spectroscopy is a very powerful tool in that with appropriate data analysis, it is often possible to characterize the different electrically-active regions in a material both qualitatively, by demonstrating their existence, and quantitatively, by measuring their individual electrical properties. It enables the overall

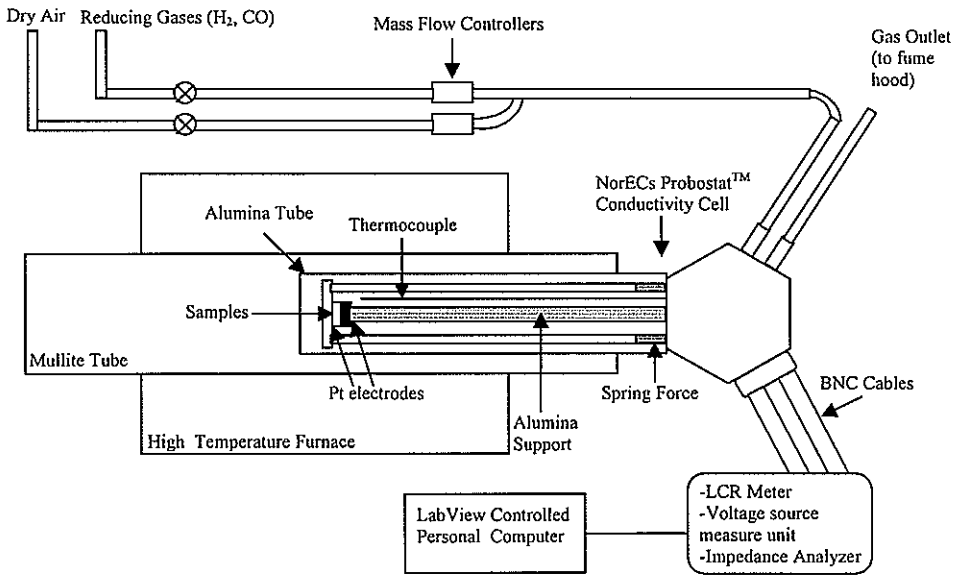

Figure 2.1: The experimental setup used for electrical measurements.

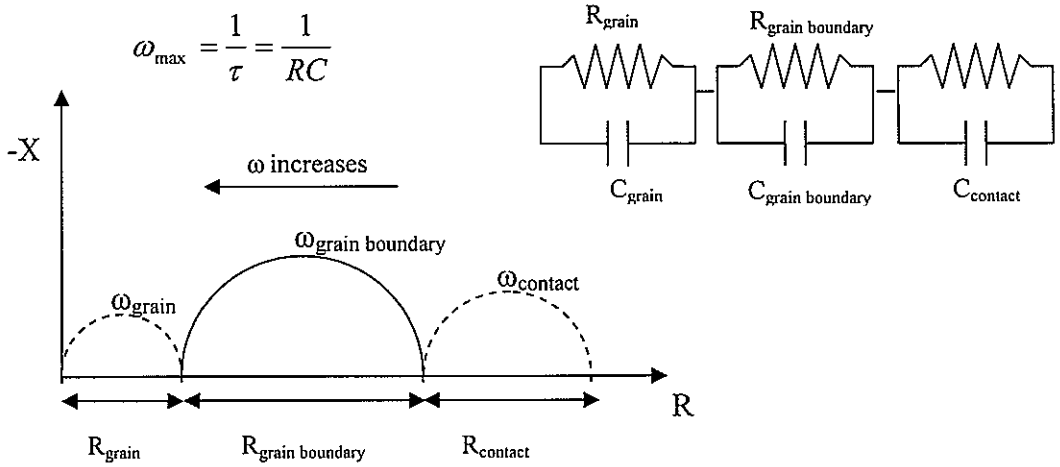

Figure 2.2: Idealized complex impedance plot and the corresponding equivalent circuit.

electrical properties of a material to be separated into their component parts, which can then be systematically studied or modified. Figure (2.2) shows a schematic, idealized impedance complex plane plot with three semicircular arcs which are modeled by its representative equivalent circuit.

Different regions of a ceramic sample are characterized by a resistance and capacitance usually placed in parallel. The characteristic relaxation time or time constant, τ, of each parallel RC element is given by the product of R and C as follows:

$$\tau = \frac{1}{\omega_{max}} = RC \tag{2.1}$$

In the frequency domain, RC elements are separable due to the relaxation shown in Equation (2.1) which holds at the frequency of maximum loss, ω_{max}, in the impedance spectrum. Therefore, it is possible to identify different RC elements and assign them to appropriate regions of the sample. The values of the individual R and C components may then be quantified.

References

1. Wagner, C., J. Chem. Phys., 1950. **18**: p. 69.
2. Hauffe, K. and H. Engell, Z. Elektrochem., 1952. **56**: p. 36.
3. Seiyama, T., et al., Anal. Chem., 1962. **34**(1502).
4. Taguchi, N. 1962, Japanese Patent Application.
5. *Figaro Engineering Inc. [Online]. Available: http://www.figarosensor.com* (date retrieved: 15 November 2004).
6. Yamazoe, N., et al., Surf. Sci., 1979. **86**: p. 335.
7. Schierbaum, K.D., U. Weimar, and W. Gopel, Sens. Actuators B, 1992. **7**: p. 709.
8. Martinelli, G. and M.C. Carotta, Sens. Actuators B, 1993. **15-16**: p. 363.
9. Martinelli, G. and M.C. Carotta, Sens. Actuators B, 1994. **18-19**: p. 720.
10. Mishra, V.N. and R.P. Agarwal, Sens. Actuators B, 1994. **21**: p. 209.
11. Gopel, W. and K.D. Schierbaum, Sens. Actuators B, 1995. **26-27**: p. 1.
12. Heilig, A., et al., Sens. Actuators B, 1997. **43**: p. 45.
13. Mukhopadhyay, A.K., et al., Ceram. Int., 2000. **26**: p. 123.
14. Salehi, A., Thin Solid Films, 2002. **416**: p. 260.
15. Gentry, S.J. and T.A. Jones, Sens. Actuators, 1986. **10**: p. 141.
16. Morrison, S.R., Sens. Actuators B, 1987. **12**: p. 425.
17. Thomas, J.M. and W.J. Thomas, *Introduction to the Principles of Heterogeneous Catalysis*. 1967, London: Academic Press.
18. Somorjai, G.A., *Principles of Surface Chemistry*. 1972, Englewood Cliffs, New Jersey: Prentice-Hall.

19. Wilson, D.M., et al., IEEE Sens. J., 2001: p. 256.
20. Takata, M., D. Tsubone, and H. Yanagida, J. Am. Ceram. Soc., 1975. **59**(1-2): p. 4.
21. Harris, L.A., J. Electrochem. Soc., 1980. **127**: p. 2657.
22. Okamoto, H., H. Obayashi, and T. Kudo, Solid State Ionics, 1980. **1**: p. 319.
23. Advani, G.J. and A.G. Jordan, J. Electron. Mater., 1980. **9**: p. 29.
24. Sermon, P.A. and G.C. Bond, Catal. Rev., 1973. **8**: p. 211.
25. Dadyburjor, D.B., Catal. Rev. Sci. Eng., 1979. **19**: p. 293.
26. Shimizu, Y. and M. Egashira, Mater. Res. Soc. Bull., 1999. **24**: p. 18.
27. Traversa, E., J. Am. Ceram. Soc., 1995. **78**(10): p. 2625.
28. Yanagida, H., Ferroelectrics, 1990. **102**: p. 251.
29. Shockley, W., Bell Syst. Tech. J., 1949. **28**: p. 435.
30. Kasap, S.O., *Principles of Electronic Materials and Devices*. 2002, New York: McGraw-Hill.
31. Anderson, R.L., Solid State Electronics, 1962. **5**: p. 341.
32. Leibovitch, M., et al., Appl. Phys. Lett., 1994. **66**(4): p. 457.
33. Nakamura, Y., et al., Chem. Lett., 1986: p. 413.
34. Nakamura, Y., et al., J. Electrochem. Soc., 1990. **137**(3): p. 940.
35. Jung, S.J., et al., J. Ceram. Soc. Jpn., 1996. **104**: p. 394.
36. Jung, S.J., et al., J. Electrochem. Soc., 1994. **141**(5): p. L53.
37. Jung, S.J. and H. Yanagida, Sens. Actuators B, 1996. **37**: p. 55.
38. Ushio, Y., M. Miyayama, and H. Yanagida, Sens. Actuators B, 1994. **17**: p. 221.
39. Baek, K.K. and H.L. Tuller, Solid State Ionics, 1995. **75**: p. 179.
40. Nakamura, Y., et al., J. Electrochem. Soc., 1998. **145**(2): p. 632.
41. Tongpool, R., C. Leach, and R. Freer, J. Mat. Sci. Letters, 2000. **19**: p. 119.
42. Baek, K.K. and H.L. Tuller, Sens. Actuators B, 1993. **13-14**: p. 238.
43. Hikita, K., M. Miyayama, and H. Yanagida, J. Am. Ceram. Soc., 1994. **77**(7): p. 1961.
44. Hikita, K., M. Miyayama, and H. Yanagida, J. Am. Ceram. Soc., 1995. **78**(4): p. 865.
45. Miyayama, M., et al., Sens. Actuators B, 1995. **24-25**: p. 383.
46. Nakamura, Y., et al., J. Catal., 1995. **153**: p. 350.
47. Nakamura, Y., et al., J. Electroceram., 1999. **4:S1**: p. 105.
48. Wolkenstein, T.H., *Advances in Catalysis*. 1960, Academic Press: New York. p. 189.
49. Traversa, E., M. Miyayama, and H. Yanagida, Sens. Actuators B, 1994. **17**: p. 257.
50. Traversa, E., et al., J. Eur. Ceram. Soc., 1998. **18**: p. 621.
51. Mitsuoka, M., A. Otofoji, and T. Arakawa, Sens. Actuators B, 1992. **9**: p. 205.
52. Makimoto, O. and T. Arakawa, Sens. Actuators B, 1993. **13-14**: p. 585.
53. Yu, J.H. and G.M. Choi, Sens. Actuators B, 1999. **61**: p. 59.

CHAPTER 3. HYDROGEN SENSITIVITY OF DOPED CuO/ZnO HETEROCONTACT SENSORS

A paper to be published in *Sensors and Actuators B*

Seymen Aygun[1,2] and David Cann[1,3]

Abstract

Heterocontact sensors based on *p*-type CuO and *n*-type ZnO ceramics have been shown to exhibit a high sensitivity to reducing gas species and an intrinsic selectivity. In this work, doped heterocontact sensors were prepared via solid state synthesis routes. CuO was doped with various monovalent (Li, Na) and isovalent (Ca, Sr, Ni) dopants at different compositions to form both single phase and two phase samples. Effects of dopants on hydrogen sensitivity through conductivity and heterogeneous microstructure were investigated using dc current-voltage measurements and ac impedance analysis. It was observed that both monovalent and divalent dopants increased the hydrogen sensitivity significantly. The highest sensitivity was observed in a 2.5 mol % Ni-CuO/ZnO heterocontact and low amounts of Li doping were shown to greatly enhance the rectifying characteristics.

KEYWORDS

hydrogen sensor, heterocontact, CuO, ZnO

[1]Graduate student and Associate Professor, respectively, Department of Materials Science and Engineering, Iowa State University.
[2]Primary researcher and author.
[3]Author for correspondence.

1. Introduction

Recently, there has been a great interest in searching for chemical sensors with novel properties, since the problems with conventional semiconductor gas sensors such as insufficient gas selectivity, inability to detect very low gas concentrations, and degradation of the sensor performance by surface contamination still persist [1,2]. The heterocontact sensor is one such system with its intelligent gas and humidity sensing properties [2,3]. The most common heterocontact system, CuO/ZnO, is unique in that it has inherent selectivity characteristics [4]. The sensing properties can be tuned to detect CO and/or H_2 gases in air by selecting the measuring frequency and the applied dc bias using an impedance analyzer. Being a capacitive-type sensor, heterocontact gas sensors can be integrated into wireless devices in which the sensor output can be converted into the frequency domain where it can be accessed remotely.

Heterocontact gas sensors detect chemical species through interactions with charge carriers at the interface. Several models have been proposed as the working mechanism for the most common heterocontact sensor, CuO/ZnO, including interface state effects [3] and preferential adsorption mechanisms in which carbon monoxide adsorbs on CuO, oxygen adsorbs on ZnO, and then the oxidation of carbon monoxide at the interface modifies the current across the junction [5]. However, a rigorous model has not yet been definitely established. There has been a focus on the detection of CO and researchers have attempted to enhance the selectivity and sensitivity through different means including increasing the density of interface states, modifying the CuO surface for stabilizing CO adsorbates, and changing the processing conditions [6-8]. Ushio *et al.* suggested that unlike most *p-n*

junctions, the interface state capacitance in CuO/ZnO junction is dominant over the depletion layer capacitance. Therefore a high density of interface states is essential for the detection of CO [6]. Nakamura *et al.* studied CO adsorption on CuO in an attempt to decrease the catalytic activity of the surface in order to form stable CO adsorbates on CuO so that these CO molecules can react with the oxygen adsorbed on ZnO instead of reacting with the adsorbed oxygen on CuO surface [8]. In addition to the CuO/ZnO system, many other different heterocontact systems, both *p-n* and *n-n*, have been studied for gas detection [9-14]. Among these systems La_2CuO_4/ZnO *p-n* heterocontact showed strong rectifying characteristics and high sensitivity towards hydrogen gas [9].

In this study, we tried to maximize hydrogen sensitivity through an examination of the effects of bulk doping in CuO on hydrogen sensing characteristics. Previously, Na-doping in CuO has been reported to show very high selectivity to CO [15], however there are no systematic studies of the effects of dopants in heterocontact sensors. In this contribution, we report the effects of bulk aliovalent and isovalent doping in CuO on hydrogen sensitivity.

2. Experimental

2.1. Sample Preparation and Phase Analyses

Polycrystalline samples of doped CuO and ZnO were synthesized via solid state methods. The powders of ZnO (Aldrich Chemical Company, 99+%), CuO (Alfa Aesar, ACS), and 1 to 4 mol % of different dopants including Li_2CO_3 (Aldrich 99+% ACS), Na_2CO_3, $CaCO_3$ (Fisher, ACS), $SrCO_3$ (99+%), and NiO (Alfa Aesar 99%) were vibratory-milled in zirconia media for 6 h. Milled powders were then dried overnight. Doped CuO powders were calcined

at 800 °C for 12 h, then re-milled and dried. After that, approximately 1 wt % PVA binder was added to the powders to aid sintering. The doped-CuO and ZnO powders were pressed into 12.7 mm diameter pellets by cold uniaxial pressing under a pressure of 100 MPa and 20 MPa, respectively. The CuO pellets were sintered at 900 °C for 24 h in air, and the ZnO pellets were sintered at 1000 °C for 3 h in air. Densities of the pellets were calculated using the Archimedes method. The pellets were polished and parallel surfaces were obtained. Both the ZnO and doped CuO pellets were 1 mm in thickness. After washing the pellets with acetone, Heraeus (C1000) silver electrodes were painted on one side of the pellets and the pellets were fired at 550 °C for 30 mins. The phase analyses of the samples were done using x-ray diffraction and scanning electron microscope.

2.2. Electrical Characterization

The electrical measurements of the *p-n* heterocontacts were made in a NorECs Probostat™ conductivity cell. The heterocontact was made by mechanically contacting CuO and ZnO pellets using the spring force of the cell. The electrical properties of the samples were measured in dry air and in H_2 (4000 ppm). Dry air (N_2:O_2 = 4:1) was used as the carrier gas for H_2. The samples were equilibrated at the measuring temperature and atmosphere for 30 mins. The flow rate was fixed at 200 mL/min. A Keithley 237 high voltage source measure unit was used for dc current-voltage measurements with an applied bias ranging from -20 to +20 V at a step of 1 V. The current values were measured 1 s after a voltage is applied. Impedance measurements were made by an HP 4194A impedance analyzer, at frequencies ranging from 100 Hz to 5 MHz under a dc bias voltage (-10 to +10 V) with the

application of an ac signal (oscillation voltage of 0.5 V) in controlled gas atmosphere at 400 °C.

3. Results and Discussions

3.1. Microstructure and Phase Analyses

Ceramics of *p*-type CuO were doped with monovalent and divalent dopants at concentrations that ranged across the solubility limit to form both single phase and two phase compositions in order to investigate the effects of second phases which may act as hydrogen adsorption sites. Both Li and Na are known to form stable hydrides and hydroxides which might facilitate this effect. The compositions and the densities of the samples are shown in Table I. Although the second phase formation for 4 mol % Li and 3.5 mol % Na doped CuO were not observed in diffraction patterns, SEM studies clearly showed the presence of a second phase. In general, the addition of isovalent dopants resulted in the formation of a second phase at lower doping levels. The phases that were observed in these compositions include Ca_2CuO_3, $Cu_3Sr_{1.75}O_{5.13}$, and NiO. The lattice parameters of monoclinic CuO did not vary significantly with doping, showing just a slight variation of less than 1%. The densities of the ZnO samples were approximately 97 % and that of pure CuO were approximately 84 %. The addition of monovalent and isovalent metals resulted in a net increase in density, however the density values of the doped samples were very close to each other and no clear trends were observed with dopant concentration. These results rule out the effects of density on the sensor response. Fig. 1 shows the SEM micrograph of a cross-section of a pure CuO/ZnO heterocontact interface at room temperature. The heterocontact was made by

mechanically contacting the ceramic pellets. The porous structure with gaps up to ~ 20 μm along the interface enabled the adsorption of gas molecules on *p* and *n*-type ceramics, and hence the detection of hydrogen gas. The grain sizes were observed to be between 4-7 μm for both samples.

3.2. Dopant Effects on Electrical Properties and Sensor Response

Fig. 2 shows the current-voltage characteristics of a pure CuO/ZnO heterocontact at 400 °C. The heterocontact exhibited rectifying characteristics due to *p-n* junction formation. The reverse current was somewhat leaky due to the minority charge carrier concentration which might have been increased by oxygen vacancies or impurities. The forward current increased exponentially when the heterocontact was positively biased, i.e. CuO (+), ZnO (-), and was enhanced in the presence of hydrogen atmosphere due to recombination reactions. Since the heterocontact interface is not uniform and the amount of contacting area varies along the interface, even though the forward current can be fit to the *p-n* junction forward current-voltage relationship, $I=I_o[\exp(eV/\eta kT)-1]$, the diode factor η was found to be unrealistically large.

Fig. 3 shows the current-voltage characteristics of alkali doped CuO/ZnO heterocontacts. As it can be seen from the plots, alkali additions to CuO greatly enhanced the sensor response. The forward current was increased with increasing Li. It can also be seen that at low levels of Li doping the reverse bias leakage current was substantially reduced. At low doping levels of Li, it is likely that Li can substitute for Cu without affecting the oxygen stoichiometry [16]. The substitution reaction can be written as:

$$Li_2O + \frac{1}{2}O_2 \xrightarrow{CuO} 2Li'_{Cu} + 2O_o^x + 2h^+$$

The holes generated via Li addition might have compensated the minority charge carrier (e^-) concentration in *p*-type CuO thereby decreasing the reverse bias leakage current. Na additions also enhanced the sensor response, however both in leakage current and in hydrogen sensitivity it had lesser effects compared to Li. Furthermore, contrary to Li doping, changing the amount of Na resulted in a slight change in the forward and reverse currents.

Complex impedance plots of 1.5 mol % Li doped CuO/ZnO heterocontacts in dry air and in 4000 ppm hydrogen atmospheres at 400 °C are shown in Fig. 4. The data were fit to the equivalent circuit originally proposed by Miyayama *et al.*, in which the bulk resistance is connected in series to the interface impedance, which is composed of a parallel resistance and capacitance elements [17]. The bulk resistance values were calculated to be very small compared to interface resistance values, therefore the semicircles were attributed to the heterocontact interface. The ac impedance plots showed a substantial decrease in resistance with increased forward bias in hydrogen atmosphere which matches well with dc current-voltage measurements. The complex impedance as a function of bias between 0 and -0.5 V were fit into the equivalent circuit given above and capacitance values were calculated from those fits. To observe changes in the junction characteristics, subsequent measurements of impedance and current-voltage behavior were repeated every 1 h over a 6 h time period. While the current-voltage behavior and the rectifying characteristics remained virtually unchanged with ~ 15 % variation in current values, plots of $1/C^2$ vs. applied bias resulted in a range of diffusion potential values between 0.6 and 1.5 V. This can be attributed to the inherent frequency dependence of the interface charge, since the capacitance values were

essentially obtained by averaging several reactance and resistance values over a range of frequencies.

The ac capacitance increased in the presence of hydrogen, which can be attributed to a modification in the concentration of charge carriers by adsorption and surface reactions of gas molecules [4]. The ratio of the capacitance in hydrogen to the capacitance in air was found to be approximately 10 over the entire range of measurement frequency 100 Hz to 5 MHz at 3 V. For example, at 100 kHz the capacitance in air was 1.4×10^{-8} F, whereas it was 1.6×10^{-7} F in hydrogen.

The effects of alkaline earth elements on the current-voltage behavior are shown in Fig. 5. Heterocontacts showed rectifying characteristics with enhanced hydrogen sensitivity compared to pure CuO/ZnO heterocontact. The addition of high concentrations of Sr resulted in an increase in the forward current. Group II metal dopants such as Sr enhance the conductivity of CuO in a manner similar to Group I metals [18]. Reverse bias leakage currents increased for both Sr and Ca doped samples. Ni doping had similar effects to alkali and alkaline earth dopants, as shown in Fig. 6. Contrary to many other dopants, an increased amount of Ni resulted in the reduced forward currents. Furthermore, high doping levels greatly suppressed the forward current in air resulting in very high hydrogen sensitivity.

4. Summary and Conclusions

Table II shows the summary of the sensitivity and leakage currents of doped CuO/ZnO heterocontacts with the sensitivity S defined as the ratio $I_{hydrogen}/I_{air}$ at 10 V. The sensitivity for the pure heterocontact was found to be the lowest with $S \approx 2.3$, and 2.5 mol %

Ni doped heterocontact showed the highest sensitivity to hydrogen $S \approx 6.2$. The Ni doped sample also showed the highest sensitivity over the bias range 0 - 20 V. It was observed that Li doping displayed the greatest effect on rectifying characteristics. With 0.5 mol % Li doping, the reverse bias leakage current at -5 V was reduced to 0.2 mA. The bias dependence of the sensitivity is shown in Fig. 7. As it can be seen, the sensitivity of the pure heterocontact remained almost constant with applied bias. The sensitivity of Ni doped sample showed a maximum at low bias values with a maximum value of $S = 9.4$ at 2 V. The sensitivity of all the other dopants showed the same trend which was characterized by an increase in S at low bias values. Above 5 V, S remained nearly constant.

Overall, the addition of monovalent and isovalent metals enhanced the hydrogen adsorption kinetics on *p*-type CuO thereby increasing the sensitivity of the heterocontact sensor. The reaction near the heterocontact interface can be simply written as:

I $O_2 + 2e^- \rightarrow 2O^-$

II $2H_2 + 4h^+ \rightarrow 4H^+$

III $4H^+ + 2O^- \rightarrow 2H_2O$

The forward current was increased in the presence of hydrogen due to the enhancement of reaction II which lowered the potential barrier at the interface. Additionally, alkali metals may act as acceptor dopants in CuO, thus increasing the hole density. At high doping levels, Group I or II metals form second phases which may act as hydrogen adsorption sites. Examples of this have been seen in many other semiconductor sensors such as SnO_2, in which Pt and Pd has been used as adsorption sites for reducing gases [19].

In conclusion, doped CuO/ZnO heterocontacts were successfully synthesized via solid state synthesis routes which exhibited rectifying behavior. Both aliovalent and isovalent

doping of CuO improved the hydrogen sensitivity through enhanced adsorption kinetics. The composition 2.5 mol % Ni doped CuO/ZnO showed the highest sensitivity to hydrogen over the bias range 0 – 20 V. The forward current was also greatly increased with Li and Sr additions. The rectifying characteristics were also enhanced with dopants, and reverse leakage bias current was greatly reduced with 0.5 mol % Li doping. Comparing single phase system with two phase system, no dramatic increase was observed in hydrogen sensitivity.

Acknowledgements

This work was supported by NASA through grant NAG-1-029-98.

References

[1] H. Yanagida, Intelligent Ceramics, Ferroelectrics 102 (1990) 251.

[2] E. Traversa, Design of Ceramic Materials for Chemical Sensors with Novel Properties, J. Am. Ceram. Soc. 78 (1995) 2625.

[3] Y. Nakamura, A. Ando, T. Tsurutani, O. Okada, M. Miyayama, K. Koumoto, and H. Yanagida, Gas Sensitivity of CuO/ZnO Hetero-contact, Chem. Lett. (1986) 413.

[4] K. Hikita, M. Miyayama, and H. Yanagida, New Approach to Selective Semiconductor Gas Sensor Using a dc-Biased *pn* Heterocontact, J. Am. Ceram. Soc. 78 (1995) 865.

[5] Y. Nakamura, H. Yoshioka, M. Miyayama, H. Yanagida, T. Tsurutani, and Y. Nakamura, Selective CO Gas Sensing Mechanism with CuO/ZnO Heterocontact, J. Electrochem. Soc. 137 (1990) 940.

[6] Y. Ushio, M. Miyayama, and H. Yanagida, Effects of Interface States on Gas-Sensing Properties of a CuO/ZnO Thin-Film Heterojunction, Sens. Actuators B 17 (1994) 221.

[7] S. J. Jung, Y. Nakamura, A. Kishimoto, and H. Yanagida, Modified CuO Surface Appropriate for Selective CO Gas Sensing at CuO/ZnO Heterocontact, J. Ceram. Soc. Jpn. 104 (1996) 394.

[8] Y. Nakamura, H. Zhuang, A. Kishimoto, O. Okada, and H. Yanagida, Enhanced CO and CO_2 Gas Sensitivity of the CuO/ZnO Heterocontact Made by Quenched CuO Ceramics, J. Electrchem. Soc. 145 (1998) 632.

[9] E. Traversa, M. Miyayama, and H. Yanagida, Gas Sensitivity of ZnO/La_2CuO_4 Heterocontacts, Sens. Actuators B 17 (1994) 257.

[10] M. Mitsuoka, A. Otofuji, and T. Arakawa, Sensing Properties of $LnMO_3/SnO_2$ (Ln = rare earth, M = Cr, Co, Mn, Fe) Having a Heterojunction, Sens. Actuators B 9 (1992) 205.

[11] O. Makimoto and T. Arakawa, Sensing Properties of Ln_2CuO_4/SnO_2 (Ln = rare earth) Having a Heterojunction, Sens. Actuators B 13-14 (1993) 585.

[12] R. Mochinaga, T. Yamasaki, and T. Arakawa, The Gas Sensing of $SmCoO_x/MO_x$ (M = Fe, Zn, In, Sn) Having a Heterojunction, Sens. Actuators B 52 (1998) 96.

[13] J. H. Yu, G. M. Choi, Electrical and CO Gas-Sensing Properties of ZnO/SnO_2 Hetero-Contact, Sens. Actuators B 61 (1999) 59.

[14] W. J. Moon, J. H. Yu, and G. M. Choi, The CO and H_2 Gas Selectivity of Cuo-doped SnO_2-ZnO Composite Sensor, Sens. Actuators B 87 (2002) 464.

[15] S. J. Jung, H. Ohsawa, Y. Nakamura, H. Yanagida, K. Hasumi, and O. Okada, Effects of Na_2CO_3 Addition on the Gas Sensing Characteristics of CuO/ZnO Heterocontact, J. Electrochem. Soc. 141 (1994) L53.

[16] X. G. Zheng, H. Yamada, D. J. Scanderberg, M. B. Maple, and C. N. Xu, Effect of Hole Doping in $Li_xCu_{1-x}O$, Phys. Rev. B 67 (2003) 214516.

[17] M. Miyayama, K. Hikita, G. Uozumi, and H. Yanagida, A.c. Impedance Analysis of Gas-Sensing Property in CuO/ZnO Heterocontacts, Sens. Actuators B 24-25 (1995) 383.

[18] S. Tanaka, Y. Sawai, A. Chiba, K. Takahashi, and Y. Saito, Ceramic Resistors Based on Copper Oxides, Key Eng. Mater. 228-229 (2002) 229.

[19] W. Gopel and K. D. Schierbaum, SnO_2 Sensors: Current Status and Future Prospects, Sens. Actuators B 26-27 (1995) 1.

Table I

Compositions and the densities of doped CuO samples. Phase analysis was obtained from a combination of XRD and SEM.

Mol % dopant	Phase Analysis	Density (g/cm^3)
Pure	Single phase	5.3
0.5 Li	Single phase	5.8
1.5 Li	Single phase	5.9
4.0 Li	Two phases	5.8
0.5 Na	Single phase	5.6
2.0 Na	Single phase	5.4
3.5 Na	Two phases	5.5
0.5 Sr	Single phase	5.9
2.5 Sr	Two phases	5.7
3.5 Sr	Two phases	5.3
1.0 Ca	Single phase	5.6
2.5 Ca	Two phases	5.6
3.5 Ca	Two phases	5.6
1.5 Ni	Single phase	5.7
2.5 Ni	Two phases	5.5
3.5 Ni	Two phases	5.5

Table II

Hydrogen sensitivity and reverse leakage bias currents of the heterocontacts. Sensitivity S is defined by the current ratio $I_{hydrogen}/I_{air}$ at 10 V. S_{max} is the maximum sensitivity over the bias range 0-20 V.

	CuO/ZnO	Li doped		Na doped		Sr doped		Ca doped		Ni doped	
Mol %	Pure	0.5	1.5	0.5	3.5	0.5	2.5	1.0	2.5	1.5	2.5
S	2.3	3.1	4.6	3.0	4.4	3.3	4.1	2.5	4.1	4.1	6.2
S_{max}	2.3	3.3	4.9	4.1	4.8	3.4	4.1	2.6	4.1	8.7	9.4
I_{sat} (mA) (H_2, -5V)	1.5	0.2	0.9	1.3	0.8	1.4	1.0	1.4	1.6	1.4	1.7

Fig. 1. SEM micrograph of a cross-section of a pure CuO/ZnO heterocontact interface.

Fig. 2. Current-voltage characteristics of pure CuO/ZnO heterocontact at 400 °C in air and 4000 ppm H_2.

Fig. 3. Current-voltage characteristics of (a) 0.5 mol % Li, (b) 1.5 mol % Li, (c) 0.5 mol % Na, and (d) 3.5 mol % Na doped CuO/ZnO heterocontacts at 400 °C in air and 4000 ppm H_2.

Fig. 4. Complex impedance plots of 1.5 mol % Li doped CuO/ZnO heterocontacts (a) in air and (b) in 4000 ppm hydrogen atmospheres at 400 °C.

Fig. 5. Current-voltage characteristics of (a) 0.5 mol % Sr, (b) 2.5 mol % Sr, (c) 1.0 mol % Ca, and (d) 2.5 mol % Ca doped CuO/ZnO heterocontacts at 400 °C in air and 4000 ppm H_2.

Fig. 6. Current-voltage characteristics of (a) 1.5 mol % Ni and (b) 2.5 mol % Ni doped CuO/ZnO heterocontacts at 400 °C in air and 4000 ppm H_2.

Fig. 7. Sensitivity of the heterocontacts as a function of applied bias at 400 °C.

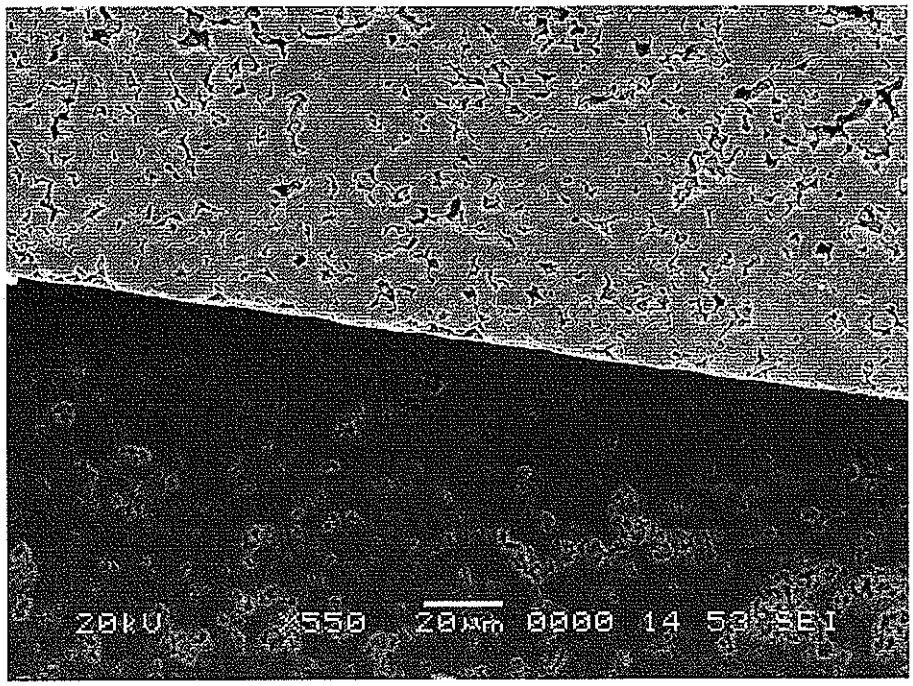

Fig. 1

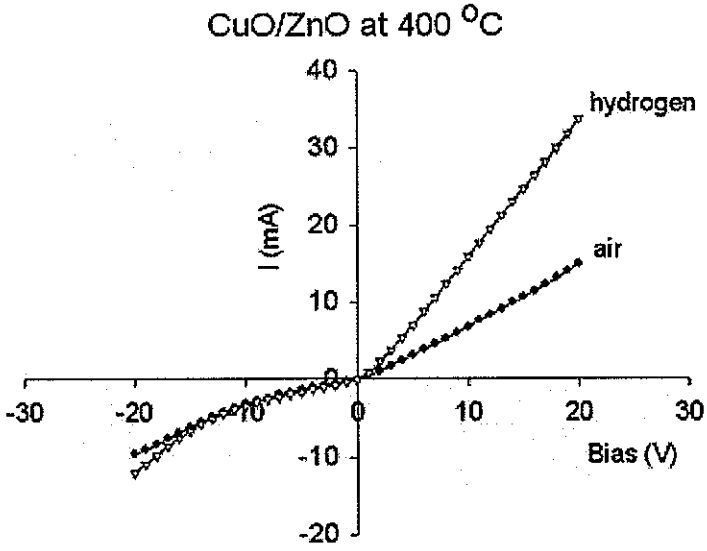
CuO/ZnO at 400 °C
40
30
20
10
0
-10
-20
-30
-20
-10
0
10
20
30
I (mA)
Bias (V)
hydrogen
air

Fig. 2.

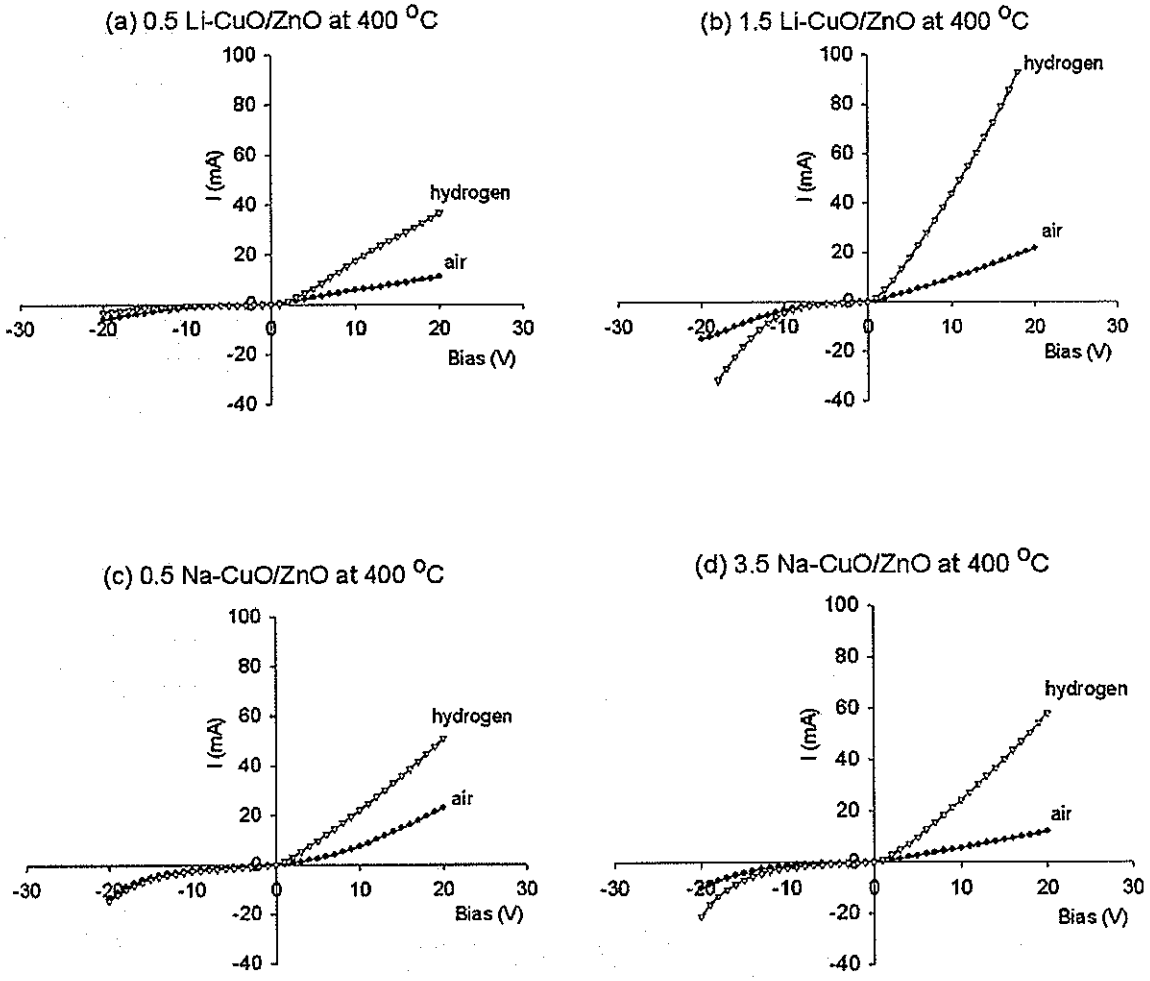
(a) 0.5 Li-CuO/ZnO at 400 °C
I (mA)
Bias (V)
hydrogen
air
(b) 1.5 Li-CuO/ZnO at 400 °C
I (mA)
Bias (V)
hydrogen
air
(c) 0.5 Na-CuO/ZnO at 400 °C
I (mA)
Bias (V)
hydrogen
air
(d) 3.5 Na-CuO/ZnO at 400 °C
I (mA)
Bias (V)
hydrogen
air

Fig. 3

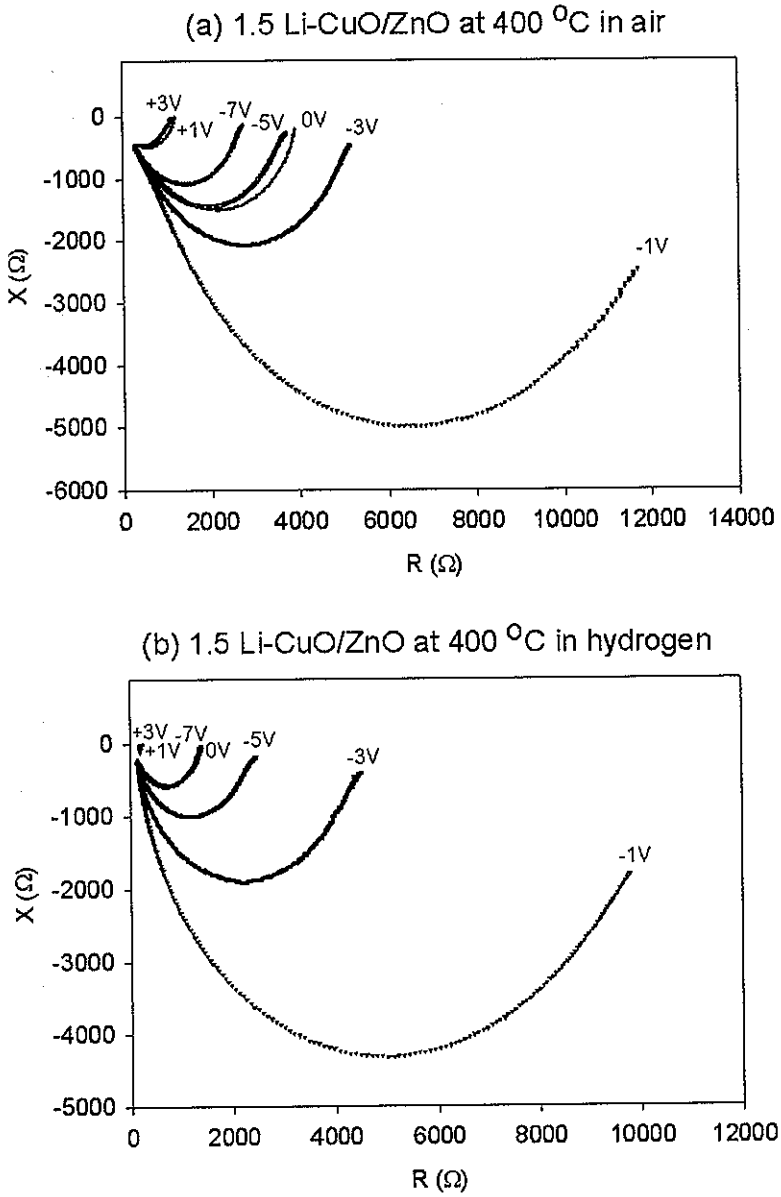
(a) 1.5 Li-CuO/ZnO at 400 °C in air
+3V
+1V
-7V
-5V
0V
-3V
-1V
X (Ω)
R (Ω)
0
-1000
-2000
-3000
-4000
-5000
-6000
0
2000
4000
6000
8000
10000
12000
14000
(b) 1.5 Li-CuO/ZnO at 400 °C in hydrogen
+3V
+1V
-7V
0V
-5V
-3V
-1V
X (Ω)
R (Ω)
0
-1000
-2000
-3000
-4000
-5000
0
2000
4000
6000
8000
10000
12000

Fig. 4

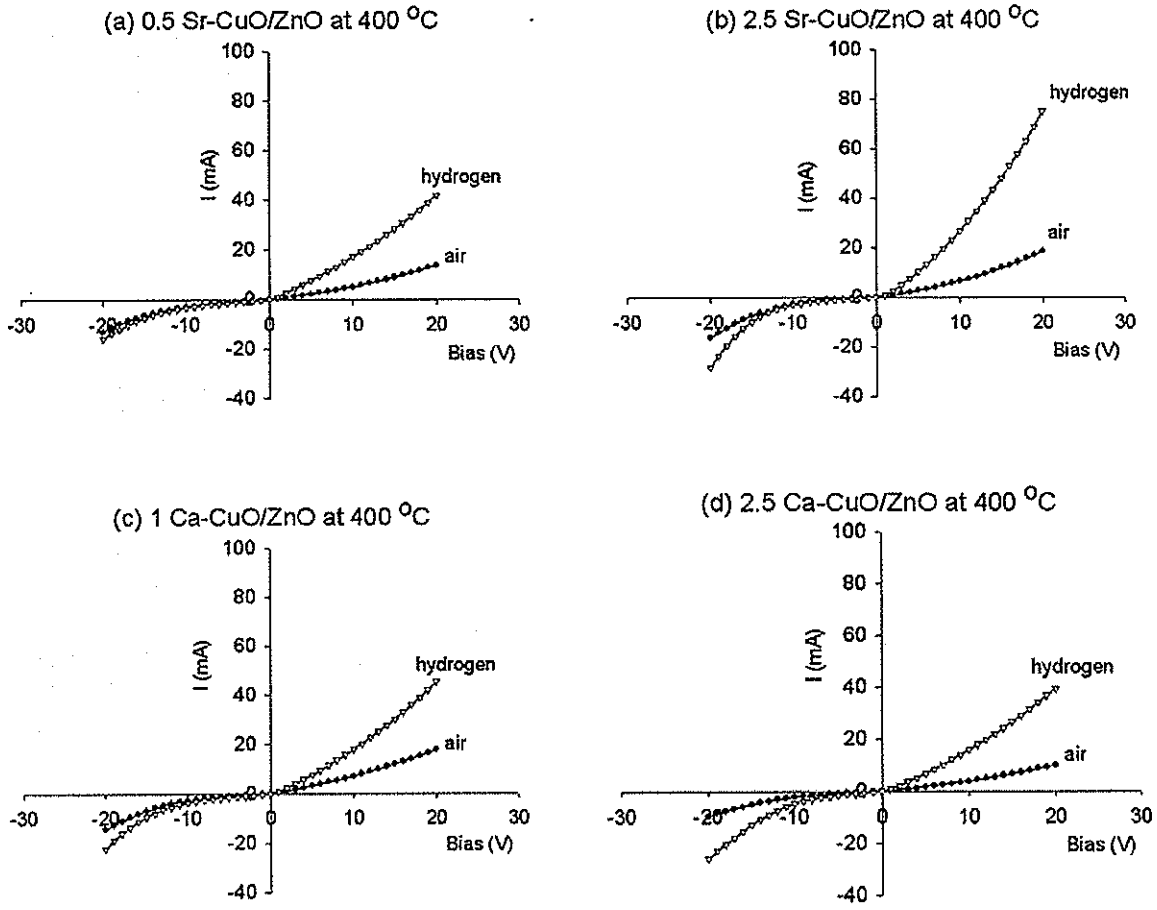
(a) 0.5 Sr-CuO/ZnO at 400 °C
(b) 2.5 Sr-CuO/ZnO at 400 °C
(c) 1 Ca-CuO/ZnO at 400 °C
(d) 2.5 Ca-CuO/ZnO at 400 °C
I (mA)
Bias (V)
hydrogen
air
100
80
60
40
20
0
-20
-40
-30
-20
-10
0
10
20
30

Fig. 5

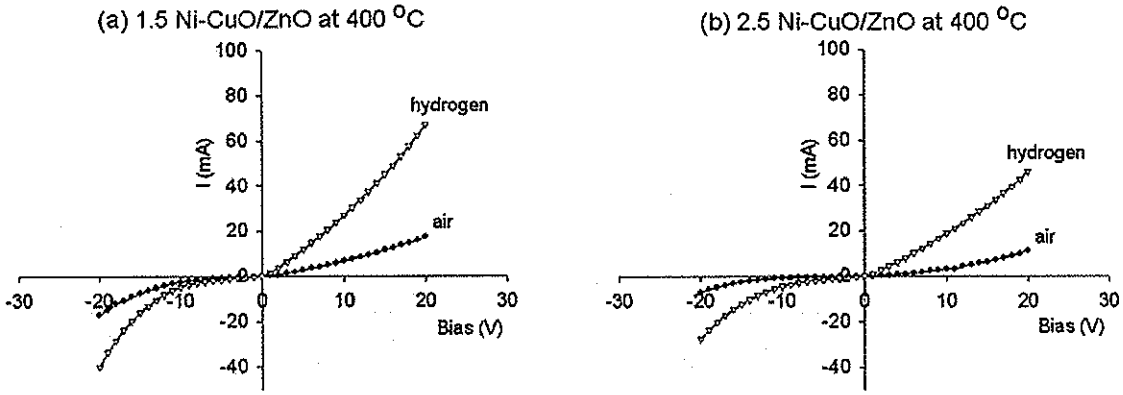
(a) 1.5 Ni-CuO/ZnO at 400 °C
100
80
60
40
20
0
-20
-40
I (mA)
hydrogen
air
-30
-20
-10
0
10
20
30
Bias (V)
(b) 2.5 Ni-CuO/ZnO at 400 °C
100
80
60
40
20
0
-20
-40
I (mA)
hydrogen
air
-30
-20
-10
0
10
20
30
Bias (V)

Fig. 6

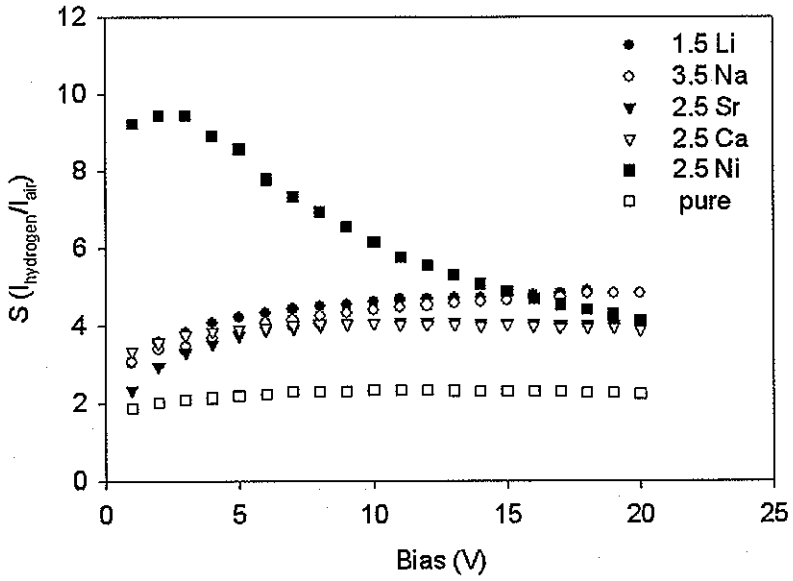
12
10
8
6
4
2
0
0
5
10
15
20
25
S (I_hydrogen/I_air)
Bias (V)
1.5 Li
3.5 Na
2.5 Sr
2.5 Ca
2.5 Ni
pure

Fig. 7

CHAPTER 4. RESPONSE KINETICS OF DOPED CuO/ZnO HETEROCONTACTS

A paper to be submitted to *Journal of Physical Chemistry B*

Seymen Aygun[1,2] and David Cann[1,3]

Abstract

In this work the effects of doping on hydrogen sensitivity and sensor response of CuO/ZnO heterocontacts were examined. Both current-voltage and current-time measurements were utilized in hydrogen/air and hydrogen/nitrogen atmospheres at 400 °C. The addition of Ni to *p*-type CuO and Ga to *n*-type ZnO were observed to enhance the sensor properties. Through analysis of the time dependent current data, it was shown that the sensor response of the heterocontact can be modeled via a two-site Langmuir adsorption model. The response times of the two sites were calculated using this model. While one of the sites showed a significant decrease in response time when the *p*-side was doped with Ni, the response time of the other site changed only slightly. The highest sensitivity was obtained by doping the *n*-side with Ga at the expense of the response rate. The fastest response times were achieved when both sides of the heterocontact were doped. This suggests that carrier density may play a significant role in the sensor response.

[1]Graduate student and Associate Professor, respectively, Department of Materials Science and Engineering, Iowa State University.
[2]Primary researcher and author.
[3]Author for correspondence.

1. Introduction

Hydrogen gas is used in a number of areas such as aeronautics, nuclear reactors, chemical processing, pharmaceuticals, and fuel cells. It also has many potential applications as a clean, efficient, and renewable energy carrier. It can be used directly for combustion, which produces much more energy than other fuels, or can be used indirectly in fuel cells to produce electricity. Furthermore, it is a non-polluting energy source with water being its only combustion product. Since it is a flammable and explosive gas, monitoring and leakage detection of hydrogen is critical in these applications. Therefore, sensors which are able to detect hydrogen at low concentrations as well as in the presence of other gases are crucial. This brings the demand for low cost, reliable, sensitive, selective hydrogen sensors.

The heterocontact sensor is one such promising candidate for gas sensing with its sensitivity and inherent selectivity characteristics. The sensor is unique in that the selectivity to a specific gaseous species can be tuned by changing the applied bias or the measuring frequency. The bulk heterocontact sensor is formed by clamping a *p*-type and an *n*-type ceramic pellet together and operates on the principle of measuring a change in interface impedance due to the adsorption of reducing gases at the interface. The sensor exhibits rectifying current-voltage behavior which is sensitive to reducing gases at positive biases. The most widely studied heterocontact system, CuO/ZnO, shows sensitivity towards many gases including H_2, CO, water vapor, H_2S, and C_2H_5OH.[1-4] It has also been shown that the frequency and/or bias dependence of the complex impedance can be used to detect gases and distinguish CO from H_2.[5] In addition to the bulk device, different forms of the heterocontact have been studied such as thin films and layered structures which improve the

reproducibility and the integrity of the sensor.[6-8] Nonetheless, it is important to note that the bulk sensors made by mechanically contacting the ceramics exhibit clear rectifying characteristics with high sensitivity towards reducing gases.

Semiconductor gas sensors work on the principle of changing their resistance with changing atmospheric composition through the reactions on the sensor surface involving gas molecules. During this change, the sensor switches from one equilibrium state (e.g. resistance in air atmosphere) to another equilibrium state (e.g. resistance in hydrogen atmosphere). Therefore, the sensitivity of a gas sensor, which is the ratio of these resistances in different atmospheres, can be studied either by comparing the sensor response at equilibrium states or analyzing the transition between these states. The former determines the magnitude of the sensor signal, whereas the latter determines the rate of the signal. Both are very important when considering a gas sensor for a particular application. To date, heterocontact research has been focused on equilibrium measurements of the CuO/ZnO system, however there have only been a few studies which include the current-time behavior of the sensor.[1,9]

The effects of dopants on the I-V characteristics of the heterocontacts has been demonstrated in our previous work.[10] In the present work, the effects Ni doping in CuO and Ga doping in ZnO on the response kinetics of the heterocontact sensor is reported. The current-time data were fit to a two-site Langmuir adsorption model and the response rates of the sites were analyzed for different compositions. The results showed that doping remarkably increased both the overall response time and the sensitivity of the sensor.

2. The Model

The barrier height of the heterocontact interface changes with the oxidation of reducing gases adsorbed on either side of the heterocontact. If we consider a simple one stage kinetic scheme, we can derive a two-site Langmuir model which relates the change in current to the surface coverage of the gas.[11-14] The oxidation reaction of a reducing gaseous species R on the surface of a heterocontact component at high temperatures can be written as

$$O^-_{ad} + R_{ad} \rightarrow RO + e^- \tag{1}$$

Here, if we assume that the adsorbed oxygen regeneration rate is negligible the current change across the interface will be proportional to the concentration of the adsorbed reducing gas.[15] Hence, the surface coverage values can be obtained from the normalized current vs. time data.

The total number of adsorbed molecules a on a surface can be written as

$$a = n_{\text{total}}\theta \tag{2}$$

where n_{total} is the number of sites and θ is the fraction of those surface sites covered. Assuming monolayer coverage, the simple Langmuir rate equation for a single adsorbate on homogeneously active sites is given by[16]

$$\frac{d\theta}{dt} = k_a(1-\theta)P_{\text{gas}} + k_d\theta \tag{3}$$

where P_{gas} is the partial pressure of the gas and k_a and k_d are the adsorption and desorption constants, respectively. By integrating Eq. (3) one obtains the relation

$$\theta = \frac{k_a P_{gas}}{k_a P_{gas} + k_d}[1 - \exp(-(k_a P_{gas} + k_d)t)] \quad (4)$$

Substituting $k_1 = k_a P_{gas}$ and $k_2 = k_a P_{gas} + k_d$ gives

$$\theta = \frac{k_1}{k_2}[1 - \exp(-k_2 t)] \quad (5)$$

If there are two types of sites, then the Eqs. (2) and (5) become

$$a = n_{total}\theta = n_1\theta_1 + n_2\theta_2 \quad (6)$$

$$\theta = \chi_1\theta_1 + \chi_2\theta_2 = \chi_1 \frac{k_1}{k_2}[1 - \exp(-k_2 t)] + \chi_2 \frac{k_3}{k_4}[1 - \exp(-k_4 t)] \quad (7)$$

where $\chi_1 = n_1 / n_{total}$, fraction of sites of type 1 and $\chi_2 = n_2 / n_{total}$, fraction of sites of type 2. Generally, the response time is defined as the time of which the coverage has reached 1/e of the final equilibrium current value. Therefore the reciprocals of the kinetic constants k_2 and k_4 are denoted as the response times for the two sites, τ_1 and τ_2, respectively.

3. Experimental

Ceramics of doped CuO and ZnO were prepared via solid state processing routes. The batches were prepared using appropriate stoichiometric amounts of powders of ZnO (Aldrich, 99+%), CuO (Alfa Aesar, ACS), Ga_2O_3 (All-Chemie, 99.999%), and NiO (Alfa Aesar 99%). After that, the powders were milled in zirconia media for 6 h and then dried overnight. Doped CuO powders were calcined at 800 °C and doped ZnO powders were calcined at 900 °C for 12 h in air. After the addition of approximately 1 wt% PVA (poly vinyl alcohol) binder, the powders were pressed into pellets by cold uniaxial pressing. The pressures for CuO and ZnO compositions were 100 and 20 MPa, respectively. The pellets of

CuO were sintered at 900 °C for 24 h in air, and the pellets of ZnO were sintered at 1000 °C for 3 h in air. The sintered pellets were ground down to a thickness of 1 mm and Heraeus (C1000) silver electrodes were painted on one side of the pellets. They were then fired at 550 °C for 30 mins. The electrical measurements of the heterocontacts were performed in a NorECs Probostat™ conductivity cell. A Keithley 237 high voltage source measure unit was used for dc current-voltage and dc current-time measurements in various atmospheres. Dry air (N_2:O_2=4:1) or N_2 was used as the carrier gas for H_2 to dilute the hydrogen to 4000 ppm. The flow rate of the gases was fixed at 200 mL/min using mass flow controllers.

4. Results and Discussion

Sensor Response of CuO/ZnO Heterocontact and the Constituent Oxides. The current-time plots of an undoped CuO/ZnO heterocontact in air/H_2 and in N_2/H_2 atmospheres at 400 °C are shown in Figure 1. When hydrogen gas was introduced into the atmosphere, the potential barrier at the heterocontact interface decreased, and therefore the current passing through the heterocontact sensor increased (Figure 1a). The increased current corresponded to sensitivity ($I_{hydrogen}/I_{air}$) of ~2.6 which is close to the value obtained from I-V measurements.[10] When the hydrogen gas was turned off, the current reverted to its original value indicating that the process is reversible. The steep initial slope of the curve obtained after shut off shows that the recovery was also quite fast. The importance of the presence of oxygen is clearly seen in Figure 1b. In the absence of oxygen the sensor response was much slower and most importantly there was no full recovery indicating a possible reduction of the sensor.

The responses of the constituent oxides were also investigated (Figure 2). As expected from Equation 1, when the oxides were exposed to hydrogen the conductivity of *p*-type CuO was decreased and that of *n*-type ZnO was increased. The response of CuO was much faster than that of ZnO, which can be attributed to the lower density of CuO. A quantitative comparison of Figures 1a & 2 shows that the resistance of the heterocontact was much larger than the sum of the resistances of the bulk constituent oxides. This indicates that the interfacial resistance was dominant over the bulk resistances. This agrees well with the ac impedance data and the proposed equivalent circuit in which the bulk resistance values were found to be much smaller than the interface resistance.[17].

The coverage vs. time plot was derived by normalizing the current vs. time data. The electrical response of the sensor is a dynamic process and when hydrogen gas is introduced the adsorption and desorption of the gas occurs simultaneously until the gas is shut off. During this process, when the number of adsorbed molecules becomes equal to the number of desorbed molecules equilibrium, and hence monolayer coverage, is achieved. The coverage vs. time plot for a CuO/ZnO heterocontact is shown in Figure 3. The data were attempted to fit to a simple single site Langmuir isotherm, however the fit was poor with an R^2 value of 0.7852. The curves were fit to the two-site model with satisfactory results with an R^2 value of 0.9930. The data suggests that there should be two energetically different adsorption sites which is consistent with our system formed by two different materials. The single pellet measurements showed that both materials were affected by hydrogen adsorption, and hence they or their interactions may stabilize two different adsorption sites at the interface. The response times of the sites, τ_1 and τ_2, were calculated using this model and

values of 45 s and 1400 s were obtained, respectively. The response rate of the second site was significantly slower than the first site affecting the overall sensor response, especially at coverage above ~0.5. The heterocontacts were doped in an attempt to increase the response rate of the second site and hence the overall response and to increase the sensitivity of the sensor.

Effects of Dopants on the Sensor Response. In our previous study, Ni doped-CuO/ZnO heterocontacts were observed to show the highest sensitivity to hydrogen among all the monovalent and isovalent dopants such as Li, Na, Sr, and Ca using current voltage measurements.[10] Therefore, Ni was selected as the dopant for CuO in this work. The current vs. time plot of a 1.5 mol % Ni-CuO/ZnO heterocontact is shown in Figure 4. As it can be seen, the current values were higher than that of the pure heterocontact with a slightly higher sensitivity of ~2.8. The data were again fit to the two-site Langmuir isotherm and the response times, τ_1 and τ_2, were obtained as 50 s and 822 s, respectively. When compared to the pure heterocontact, τ_1 changed slightly whereas there was a dramatic decrease in τ_2. This resulted in attaining higher coverage values at smaller response times.

Doping of the *n*-type ZnO constituent was also examined. Both acceptor (Li) and donor (Ga) dopants were used. Figure 5a shows the I-V characteristics of a CuO/1.5 mol % Li doped ZnO heterocontact. The heterocontact did not show rectifying characteristics and the current values were on the order of microamperes. The loss of rectifying behavior suggests that the *p-n* junction was degraded. The large reverse bias (saturation) currents suggest a large minority carrier concentration was present in ZnO which can be attributed to the holes provided by the acceptor Li. The current vs. time response of the heterocontact was also

different than the other samples (Figure 5b). The overall response was very slow and the slowly increasing part of the response curve might be an indication of bulk effects in addition to surface adsorption. Contrary to Li doping, Ga doping had a substantial impact on the sensitivity and on the sensor response and the CuO/1.5 mol% Ga-ZnO heterocontact showed the highest sensitivity among all the samples in this work. The I-V plot shows well-defined rectifying characteristics, as shown in Figure 6a, with very high forward currents especially in the presence of hydrogen. In fact, the response in hydrogen exceeded the current range of our instrumentation above a bias of 0.8 V. The energy-band diagram which was proposed by Baek *et al.*[7] suggests that the potential barrier that electrons must overcome is much smaller than that of holes. Therefore, the current through the heterocontact will be dominated by electrons. This can explain the large increase in the forward currents by donor doping the *n*-type ZnO. The sensitivity obtained from current-time measurements (figure 6b) was also the highest with a value of ~8.2. The response times, τ_1 and τ_2, were calculated as 58 s and 1372 s. When we compare these values with the ones obtained from the pure CuO/ZnO heterocontact, it was noted that the response times of both sites were similar ($\tau_{1pure} \sim \tau_{1doped}$ and $\tau_{2pure} \sim \tau_{2doped}$). Yet the sensitivity increased significantly. Finally, to investigate a possible synergistic effect of doping both *p* and *n*-type materials, the current-time measurements for a 1.5 mol % Ni-CuO/1.5 mol % Ga-ZnO heterocontact was performed (Figure 7). The current values were observed to be in between that of the 1.5 mol % Ni-CuO/ZnO and CuO/1.5 mol % Ga-ZnO samples. The sensitivity of the heterocontact was also in between with a value of ~5.1. The synergistic effect was clearly observed in the rate

of the sensor response with τ_1 and τ_2 of 44 s and 693 s showing the quickest responses for both site 1 and site 2.

5. Summary and Conclusions

The sensitivities, the response times of site 1 and 2, and the overall response of the sensors are summarized in Table 1. The overall responses of the heterocontacts are designated by $t_{0.7}$, $t_{0.8}$, and $t_{0.9}$ which are defined as the time required for the sensor to reach a surface coverage of 0.7, 0.8, and 0.9, respectively. As can be seen from the data, doping the *p*-side resulted in significant decrease in the response time of site 2, while site 1 changed only slightly. Doping the *n*-side decreased the response rate of the sensor, however the sensitivity was substantially increased. The coverage vs. time plots of the heterocontacts are compared in Figure 8. The overall response of the sensor at 90 % coverage, $t_{0.9}$, was lowered by a factor of 4 with the synergistic effects of doping both sides of the heterocontact. Even though the response kinetics of the Ga-doped heterocontact was the slowest, it is important to keep in mind that the sensor reached very high sensitivity values within that time.

In conclusion, hydrogen sensors based on CuO/ZnO heterocontacts were successfully produced and both the sensitivity and the response kinetics of the sensor were enhanced by doping. The kinetics data were fit to a two-site Langmuir adsorption isotherm indicating that the adsorption process takes place on two energetically different sites. Doping the *p*-type side was observed to modify the response rate of one of the sites, while changing the other site only slightly. Doping the *n*-side resulted in the highest sensitivity with a value of ~8.2. The synergistic effect of doping both *p* and *n*-sides resulted in reaching surface coverage of 70 %

in slightly more than a minute. This suggests that carrier density plays a significant role in the adsorption processes, and hence in the sensor response.

Acknowledgments

This work was supported by NASA through grant NAG-1-029-98.

References and Notes

(1) Nakamura, Y.; Ando, A.; Tsurutani, T.; Okada, O.; Miyayama, M.; Koumoto, K.; Yanagida, H. *Chem. Lett.* **1986**, 413.
(2) Nakamura, Y.; Yoshioka, H.; Miyayama, M.; Yanagida, H. *J. Electrochem. Soc.* **1990**, *137*, 940.
(3) Toyoshima, Y.; Miyayama, M.; Yanagida, H.; Koumoto, K. *Jpn. J. Appl. Phys.* **1983**, *22*, 1933.
(4) Hu, Y.; Zhou, X.; Han, Q.; Cao, Q.; Huang, Y. *Mater. Sci. Eng. B* **2003**, *99*, 41.
(5) Hikita, K.; Miyayama, M.; Yanagida, H. *J. Am. Ceram. Soc.* **1995**, *78*, 865.
(6) Ushio, Y.; Miyayama, M.; Yanagida, H. *Sens. Actuators B* **1994**, *17*, 221.
(7) Baek, K. K.; Tuller, H. L. *Solid State Ionics* **1995**, *75*, 179.
(8) Nakamura, Y.; Watanabe, K.; Jung, S. J.; Osawa, H.; Yoshioka, H.; Yanagida, H. *J. Catal.* **1995**, *153*, 350.
(9) Jung, S. J.; Yanagida, H. *Sens. Actuators B* **1996**, *37*, 55.
(10) Aygun, S.; Cann, D. *Sens. Actuators B* (in press).
(11) Liu, C. J.; Hsieh, J. C.; Ju, Y. H. *J. Vac. Sci. Technol. A* **1996**, *14*, 753.
(12) Manno, D.; Micocci, G.; Serra, A.; Giulio, M. D.; Tepore, A. *J. Appl. Phys.* **2000**, *88*, 6571.
(13) Chaudhary, V. A.; Mulla, I. S.; K., V.; Hegde, S. G.; Srivinas, D. *J. Phys. Chem. B* **2001**, *105*, 2565.
(14) Ho, K. C.; Tsou, Y. H. *Sens. Actuators B* **2001**, *77*, 253.
(15) Wlodek, S.; Colbow, K.; Consadori, F. *Sens. Actuators B* **1991**, *3*, 123.
(16) Masel, R. I. *Principles of Adsorption and Reaction on Solid Surfaces*; John Wiley &Sons, Inc: New York, 1996.
(17) Miyayama, M.; Hikita, K.; Uozumi, G.; Yanagida, H. *Sens. Actuators B* **1995**, *24-25*, 383.

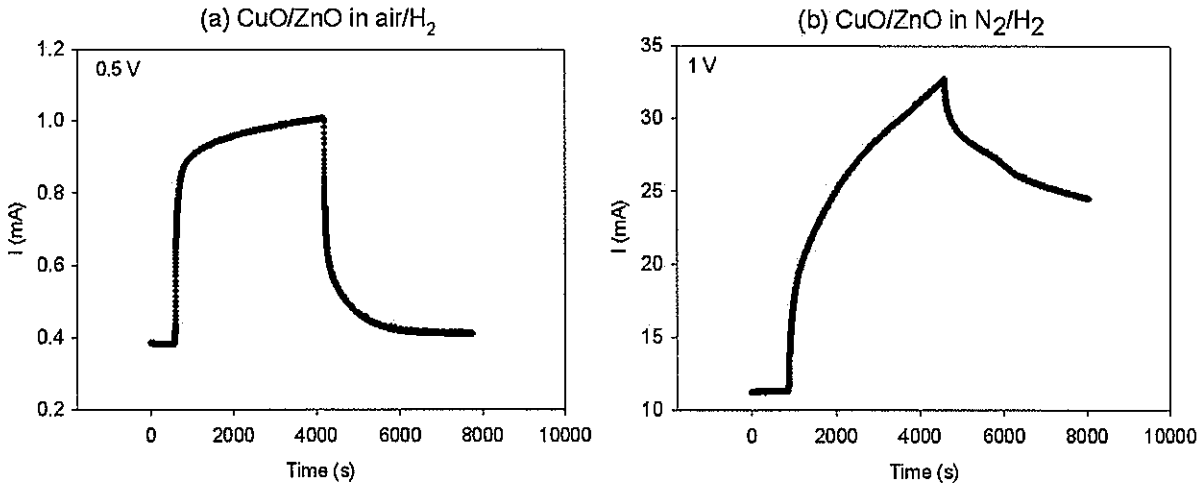

Figure 1. Current-time response of (a) CuO/ZnO in air/H_2 and (b) CuO/ZnO in N_2/H_2 at 400 °C.

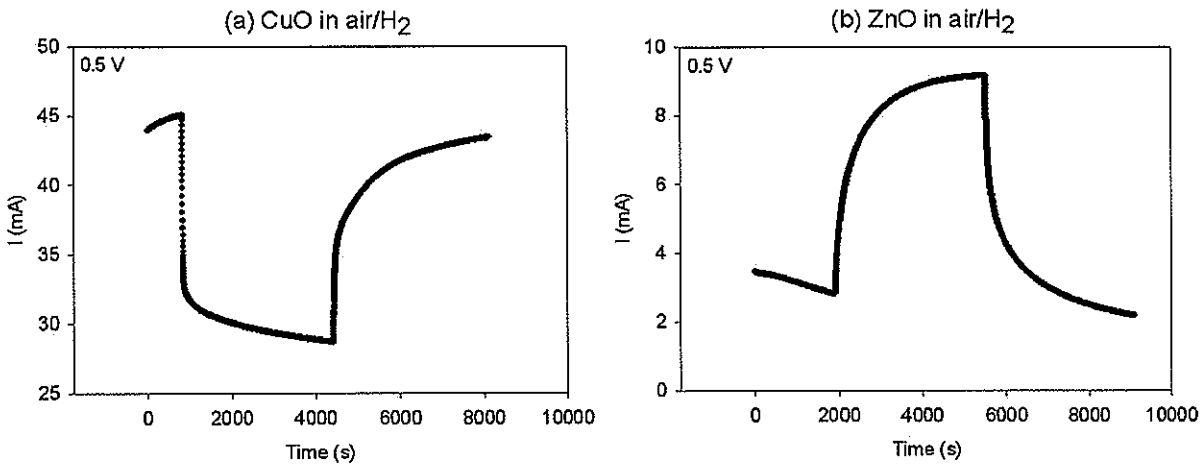

Figure 2. Current-time response of (a) CuO in air/H_2 and (b) ZnO in air/H_2.

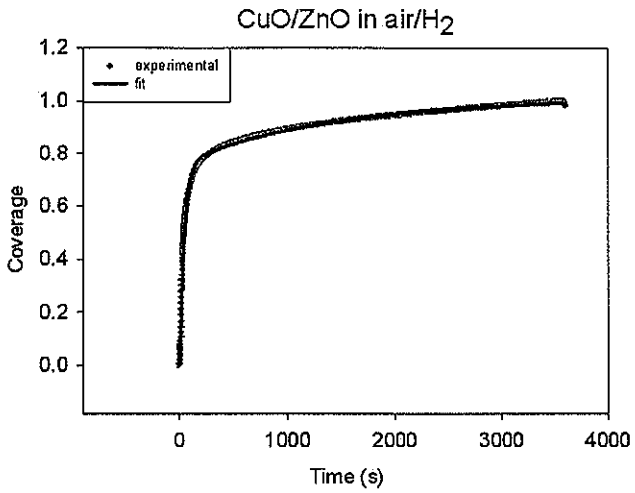

Figure 3. Coverage vs. time plot for CuO/ZnO in air/H_2 and the two-site fit.

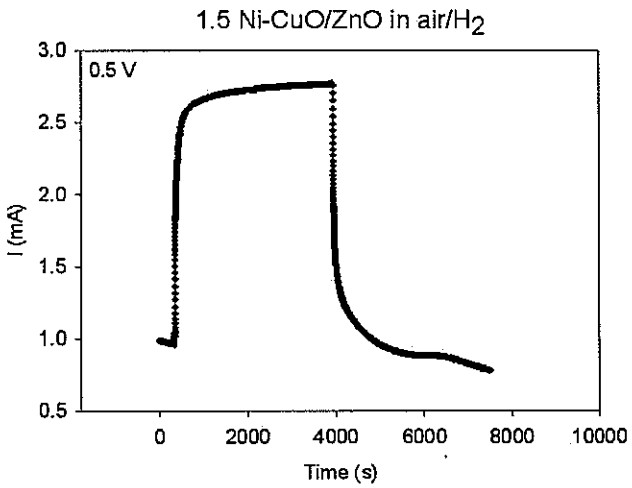

Figure 4. Current-time response of 1.5 mol % Ni-CuO/ZnO in air/H_2.

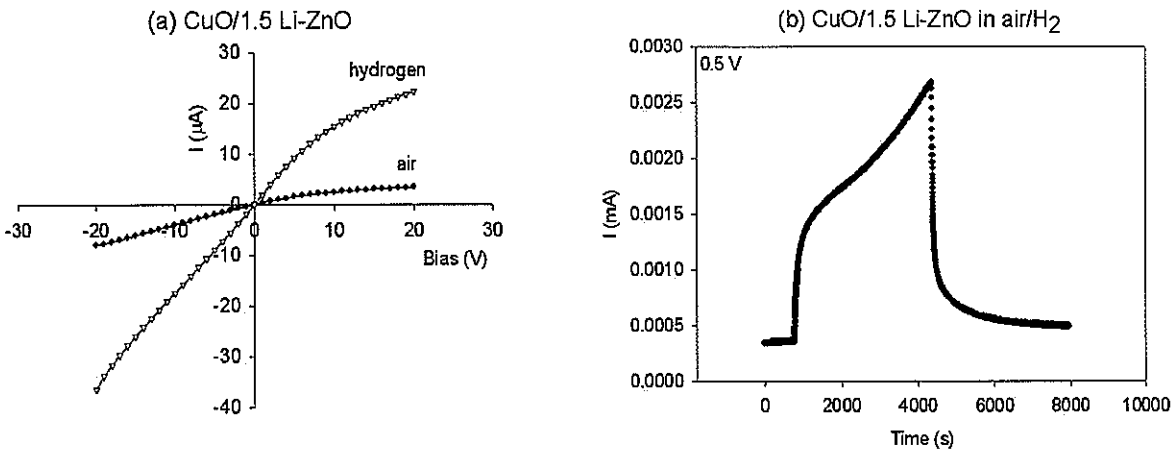

Figure 5. (a) Current-voltage plot for CuO/1.5 mol % Li-ZnO and (b) current-time response of CuO/1.5 mol % Li-ZnO in air/H_2.

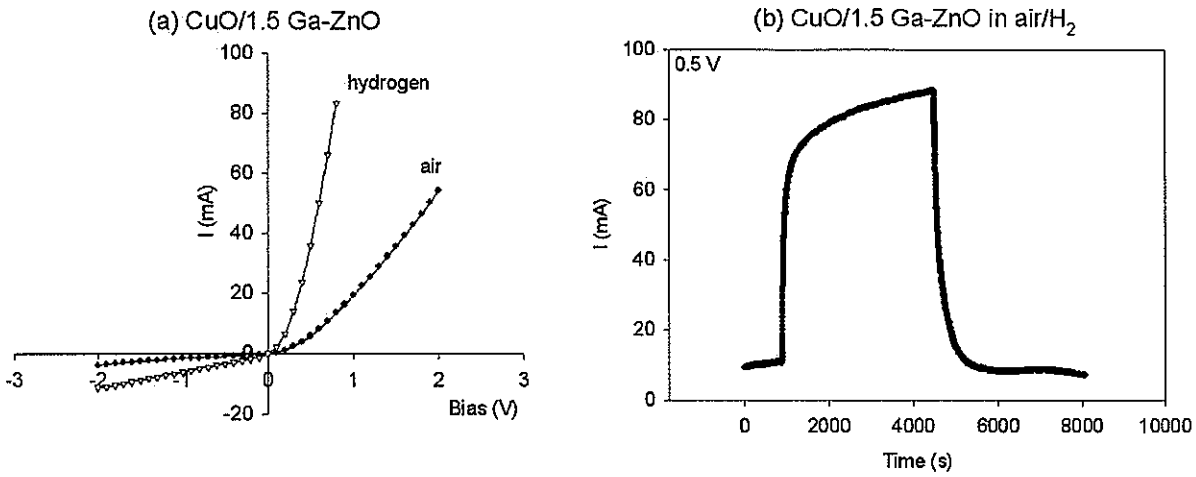

Figure 6. (a) Current-voltage plot for CuO/1.5 mol % Ga-ZnO and (b) current-time response of CuO/1.5 mol % Ga-ZnO in air/H_2.

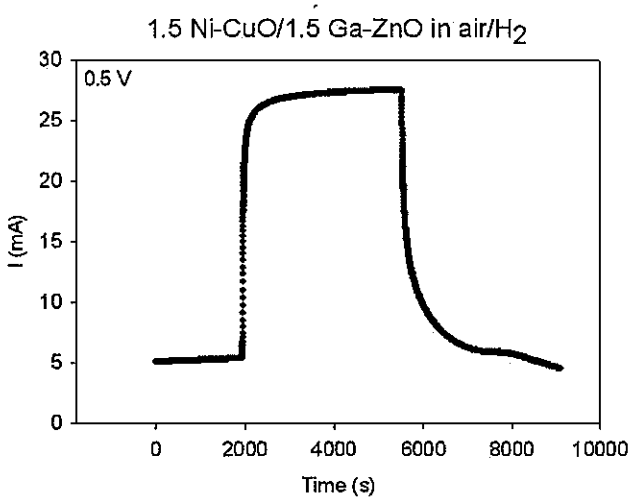

Figure 7. Current-time response of 1.5 mol % Ni-CuO/1.5 mol % Ga-ZnO in air/H_2.

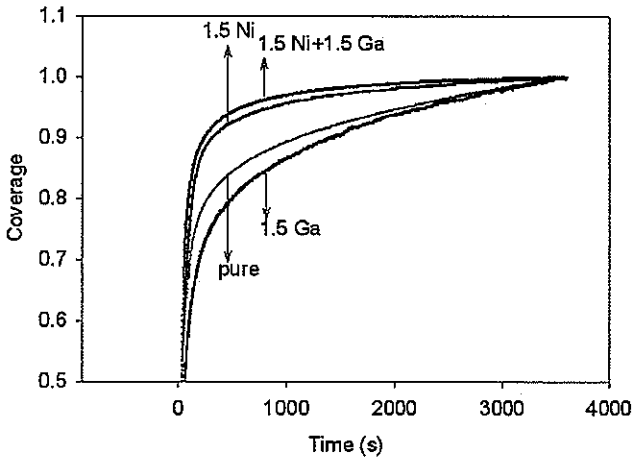

Figure 8. Coverage vs. time plots of the pure and the doped heterocontacts.

Table 1. Sensitivity, response times of the sites, and overall response times for various compositions.

	Sensitivity	τ_1 (s)	τ_2 (s)	$t_{0.7}$ (s)	$t_{0.8}$ (s)	$t_{0.9}$ (s)
CuO/ZnO	2.6	45	1400	100	216	818
1.5 Ni-CuO/ZnO	2.8	50	822	81	121	308
CuO/1.5Ga-ZnO	8.2	58	1372	171	524	1384
1.5 Ni-CuO/1.5Ga-ZnO	5.1	44	693	67	98	203

CHAPTER 5. GENERAL CONCLUSIONS

Ceramic *p-n* heterocontacts based on CuO/ZnO were successfully synthesized and a systematic study of their hydrogen sensitivity was conducted. The sensitivity and response rates of CuO/ZnO sensors were studied utilizing current-voltage, current-time, and impedance spectroscopy measurements. The heterocontacts showed well-defined rectifying characteristics and were observed to detect hydrogen via both dc and ac measurements. Surface coverage data were derived from current-time measurements which were then fit to a two-site Langmuir adsorption model quite satisfactorily. The fit suggested that there should be two energetically different adsorption sites in the system.

The Langmuir rate equation for a single adsorbate on a two-site system is given by

$$\theta = \chi_1\theta_1 + \chi_2\theta_2 = \chi_1 \frac{k_1}{k_2}[1-\exp(-k_2 t)] + \chi_2 \frac{k_3}{k_4}[1-\exp(-k_4 t)]$$

where θ is the surface coverage, χ_1 and χ_2 are the fractions of site 1 and 2, respectively, k_1 and k_2 are the kinetic constants for site 1 and k_3 and k_4 are the kinetic constants for site 2. Here, the constants k_2 and k_4 give the individual response rates of the sites, whereas the equation is used to calculate the overall response time of the sensor for a specific surface coverage value.

The heterocontacts were doped in an attempt to increase the sensitivity and the response rate of the sensor. First, the effects of doping the *p*-type (CuO) on the sensor characteristics were investigated. Doping the *p*-type CuO with both acceptor and isovalent dopants greatly improved the hydrogen sensitivity. The sensitivity of pure heterocontact observed via I-V measurements was increased from ~2.3 to ~9.4 with Ni doping. Dopants also enhanced the rectifying characteristics of the heterocontacts. Small amounts of Li

addition were shown to decrease the reverse bias (saturation) current to 0.2 mA at a bias level of -5V. No unambiguous trends were observed between the sensitivity, the conductivity, and the density of the samples. Comparing the two phase microstructure to the single phase microstructure there was no dramatic increase in the sensitivity. Kinetic studies also confirmed the improved sensor characteristics with doping. The dopants decreased the response time of the sensor by decreasing the response time of one of the adsorption sites. The *n*-type ZnO was doped with both acceptor and donor dopants. Li doping resulted in the degradation of the *p-n* junction and the response time of the sensor. However, the current-voltage behavior of Ga-doped heterocontacts showed the best rectifying characteristics with very high forward currents. Ga doped heterocontacts showed the highest sensitivity observed during current-time measurements as well, even though the sensor response was rather slow. Finally, a possible synergistic effect of doping both *p* and *n*-sides was studied by utilizing current-time measurements for 1.5 mol % Ni-CuO/1.5 mol % Ga-ZnO heterocontact. A sensitivity value of ~5.1 was obtained with the fastest response among all the samples. The time needed to reach 90 % coverage was lowered by a factor of 4 when compared to the pure heterocontact and the time needed to reach 70 % coverage was just over one minute.

Heterocontact gas sensors are promising candidates for high temperature sensor applications. Today, Si-based microelectromechanical system (MEMS) technology has shown great promise for developing novel devices such as pressure sensors, chemical sensors, and temperature sensors through complex designs. However, the harsh thermal, vibrational, and corrosive environments common to many aerospace applications impose severe limitations on their use. Sensors based on ceramic *p-n* heterocontacts are promising

alternatives because of their inherent corrosion resistance and environmental stability. The other advantages include their inherent tuning ability to differentiate between different reducing gases and a possible cost efficient production of a wireless sensor. Being a capacitive type sensor, its output can be transformed into a passive wireless device by creating a tuned LC circuit. In this way, the sensor output (the capacitance) can be accessed remotely by measuring the resonant frequency. The relatively simple structure of heterocontacts makes it suitable for thick film fabrication techniques to make sensor packages.

ACKNOWLEDGEMENTS

I would like to acknowledge many people who have helped me throughout this work. I would first like to thank my major professor Dr. David Cann, for the opportunities and the support he has given me throughout this work. The BBQ's, foosball tournaments, and trips will always be remembered. I would also like to thank my committee members, Dr. Keith Woo, Dr. Xiaoli Tan, and Dr. Rohit Trivedi for their suggestions in this work.

I would like to thank to the members of Materials Analysis Research lab, and Ozan Ugurlu for their help in XRD and SEM studies. I would also like to thank Baris Unal for the discussions on kinetic studies. Thanks to Carmen, Lynne, and Krista for their tremendous patience with my questions and needs. I will not forget Carmen's delicious salsas.

I must thank my group members Bruce, Nate, Meagen, Seunghwa, Chien-Chih, Wanwilai, Athipong, and of course the Thai godfather Naratip for their help throughout my work. I would like to thank Bruce and Melbs for many late nights, tailgates, and their support to keep me sane in Ames.

A very special thank goes to Tuğba for her constant support and endless patience through the years we spent at ISU.

Finally, I must thank my family, Zeynep, Sezer, and Baykut, and my aunt Leman, for their constant love and support. I could not have accomplished what I have had without you. I am truly thankful.